THEORETICAL AND EXPERIMENTAL EVALUATION OF CHEMICAL REACTIVITY

A Dissertation

by

QINGSHENG WANG

Submitted to the Office of Graduate Studies of
Texas A&M University
in partial fulfillment of the requirements for the degree of

DOCTOR OF PHILOSOPHY

August 2010

Major Subject: Chemical Engineering

THEORETICAL AND EXPERIMENTAL

EVALUATION OF CHEMICAL REACTIVITY

A Dissertation

by

QINGSHENG WANG

Submitted to the Office of Graduate Studies of
Texas A&M University
in partial fulfillment of the requirements for the degree of

DOCTOR OF PHILOSOPHY

Approved by:

Chair of Committee,	M. Sam Mannan
Committee Members,	Daniel F. Shantz
	Zhengdong Cheng
	Michael B. Hall
Head of Department,	Michael Pishko

August 2010

Major Subject: Chemical Engineering

ABSTRACT

Theoretical and Experimental Evaluation of Chemical Reactivity. (August 2010)

Qingsheng Wang, B.S.; M.S., Zhejiang University

Chair of Advisory Committee: Dr. M. Sam Mannan

Reactive chemicals are presented widely in the chemical and petrochemical process industry. Their chemical reactivity hazards have posed a significant challenge to the industries of manufacturing, storage and transportation. The accidents due to reactive chemicals have caused tremendous loss of properties and lives, and damages to the environment. In this research, three classes of reactive chemicals (unsaturated hydrocarbons, self-reacting chemicals, energetic materials) were evaluated through theoretical and experimental methods.

Methylcyclopentadiene (MCP) and Hydroxylamine (HA) are selected as representatives of unsaturated hydrocarbons and self-reacting chemicals, respectively. Chemical reactivity of MCP, including isomerization, dimerization, and oxidation, is investigated by computational chemistry methods and empirical thermodynamic–energy correlation. Density functional and *ab initio* methods are used to search the initial thermal decomposition steps of HA, including unimolecular and bimolecular pathways. In addition, solvent effects are also examined using water cluster methods and Polarizable Continuum Models (PCM) for aqueous solution of HA.

The thermal stability of a basic energetic material, Nitroethane, is investigated through both theoretical and experimental methods. Density functional methods are employed to explore the initial decomposition pathways, followed by developing detailed reaction networks. Experiments with a batch reactor and *in situ* GC are designed to analyze the distribution of reaction products and verify reaction mechanisms. Overall kinetic model is also built from calorimetric experiments using an Automated Pressure Tracking Adiabatic Calorimeter (APTAC).

Finally, a general evaluation approach is developed for a wide range of reactive chemicals. An index of thermal risk is proposed as a preliminary risk assessment to screen reactive chemicals. Correlations are also developed between reactivity parameters, such as onset temperature, activation energy, and adiabatic time to maximum rate based on a limited number, 37 sets, of Differential Scanning Calorimeter (DSC) data. The research shows broad applications in developing reaction mechanisms at the molecular level. The methodology of reaction modeling in combination with molecular modeling can also be used to study other reactive chemical systems.

DEDICATION

To my wife Jiejia, Mom, Daddy, Mother-in-law and Father-in-law for all their love and support.

To my professors, Dr. M. Sam Mannan and Dr. F. Albert Cotton for all their guidance and support.

ACKNOWLEDGEMENTS

I would like to thank my advisor, Dr. Sam Mannan, for all his guidance, encouragement, assistance and support throughout my Ph.D. research and education. I also would like to thank my committee members, Dr. Dan Shantz, Dr. Zhengdong Cheng, and Dr. Mike Hall, for taking time to serve on my committee. Thanks also go to all the current and previous students/staff of the Mary Kay O'Connor Process Safety Center (MKOPSC), especially Valerie Green, Donna Startz, Mary Cass, Dr. Hans Pasman, Dr. Maria Papadaki, Dr. Steven Zhang, and Dr. Dedy Ng.

I learned a lot from my previous advisor, Dr. F. Albert Cotton, through day to day conversation and discussions, and would like to express my sincere gratitude to him. I have learned to be a better scientist. I thank all members of the Laboratory for Molecular Structure and Bonding (LMSB), especially Dr. Carlos A. Murrilo (Now program director at NSF), Dr. Hong-Cai Zhou, Ms. Julie Zercher, Dr. Zhong Li, Dr. Qinliang Zhao, Mr. Jiayi Jin, and Dr. Mark Young.

I truly appreciate the help and support from my uncle, Dr. Rizhi Wang. It was a nice visit to Chemical Engineering and Materials Engineering Departments at the University of British Columbia. I would like to thank the Texas A&M Supercomputing Facility for computer time, and Dr. Lisa Perez for her help with molecular modeling.

Finally, thanks to my mother and father for their encouragement, and to my wife for her patience and love.

TABLE OF CONTENTS

LIST OF FIGURES

FIGURE Page

LIST OF TABLES

CHAPTER I

INTRODUCTION

Appropriate assessment of reactive hazards has been a significant concern in the chemical process industry. The U. S. Chemical Safety and Hazard Investigation Board (CSB) reported 167 reactive chemical incidents between 1980 and 2001, resulting in an average of five fatalities annually.[1]

The following classes of reactive materials were included in the CSB report: self-reacting chemicals, chemicals that react with common contaminants, and energetic materials. The energy initially produced by these chemicals may accelerate the reaction, which is too rapid to be controlled. These reactions can be the cause of catastrophic events because the sudden energy release can cause damage and injury from direct effects of high temperature and pressure and can cause illness and death from the release of toxic materials.

The lack of accurate knowledge about the reactive chemistry of reactants, intermediates and products has been one of major causes of these incidents.[2] Therefore, to prevent the similar incidents, it is urgent for chemists and chemical engineers to recognize chemical reactivity of these chemicals and apply this knowledge effectively in the design, operation, and maintenance of chemical processes.

This dissertation follows the style of *Industrial & Engineering Chemistry Research*.

Hazardous chemical reactivity is any chemical reaction with the potential to exhibit rates of increase in temperature and/or pressure too high to be absorbed by the environment surrounding the system. It is well known that chemical reactivity information can be obtained from literature sources or calorimetric techniques in the laboratory. Much of the traditional approach to process safety is based on controlling the hazards associated with chemical processes and plants.[3] This is done through improving operating procedures, installing safety interlocks, and improving emergency response. However, until the reactivity of chemicals is completely evaluated, it is not possible to reduce the risk of processes.[4]

There have been numerous studies on chemical reactivity so far by our Center as well as other research groups.[5,6] Usually, reactive system screening tool (RSST) or differential scanning calorimeter (DSC) are used for preliminary analysis and automated pressure tracking adiabatic calorimeter (APTAC) is used for a more detailed characterization of the temperature and pressure profiles of hazardous reactions.

These calorimetric studies have provided some information on different classes of reactive chemicals, such as organic peroxides, unsaturated hydrocarbons, and nitro compounds. However, not much effort has been devoted to the micro-scale mechanisms of the reaction systems. The mechanism and kinetic study of thermal decomposition always attracts the interest of both chemical engineers and materials scientists because it is essential to engineering safety design and fundamental to the design and optimization of materials.[7]

The objective of this research is to develop reaction mechanism to evaluate chemical reactivity for different classes of reactive chemicals, expedite hazard assessment, and find applications to process safety. This research seeks to an evaluation method through theoretical and experimental tools, and will lead to following fundamental outcomes for certain reactive chemicals: developing possible reaction pathways and determining reaction mechanisms; elucidating thermo-kinetic behaviors through calorimetric experiments and theoretical simulations; developing guidance or index as a screening tool to recognize more hazardous chemicals.

Chapter II discusses chemical reactivity evaluation methods using quantum mechanics calculation and experimental measurements. Three highly reactive systems are investigated for evaluating chemical reactivity. In Chapter III, the runaway reactions of methylcyclopentadiene (MCP) are presented. This system represents an important class of unsaturated hydrocarbons which are widely used in the manufacturing of polymers. The second reactive system, presented in Chapter IV, is the decomposition pathways of hydroxylamine (HA), which represents self-reacting chemicals. The decomposition of energetic materials (EM) is the third system evaluated and is presented in Chapter V.

Finally in Chapter VI, an index of thermal risk is developed as a preliminary risk assessment to screen reactive chemicals, followed by conclusions as Chapter VII.

CHAPTER II

REACTIVITY EVALUATION APPROACHES

Effective identification, understanding, and evaluation of reactive chemical hazards in process chemistry are critical components for optimal and safe process operation. Many approaches have been suggested to identify, categorize, and evaluate chemical reactivity before.[8] However, because the needs for an assessment procedure vary from one chemical process to another, much effort was to provide specific-case assessment approaches.[9] As we know, many methodologies cannot be generalized to other chemical reactivity evaluations. However, any reactive chemicals could be analyzed for their fundamental properties using both theoretical and experimental methods. In this chapter, brief introductions of these two basic approaches are addressed.

1. Theoretical Approaches

In runaway reactions, we care about how much energy will be released and how fast the energy is released. Therefore, both thermodynamic and kinetic information are important to evaluate chemical reactivity. From theoretical point of view, thermodynamic properties, such as heat of reaction, can be calculated from the molecular structures; while kinetic properties, such as activation energy, can be obtained from transition state theory calculations. Both thermodynamic and kinetic properties could be modeled by using computational quantum chemistry method [10] via well developed software (i.e., Gaussian03).[11]

1.1 An Overview of Computational Chemistry

Computational chemistry simulates chemical structures and reactions numerically, based on the fundamentals of physics. It allows chemists or chemical engineers to study chemical phenomena by running calculations on computers, and provides information which may be impossible to obtain through experiments or observations.

There are two broad areas within computational chemistry: molecular mechanics and electronic structure theory. Both of them can perform geometry optimization and calculate energy of molecules. However, molecular mechanics simulations use the laws of classical physics (i.e., fore field) to predict the structures and properties of molecules. Electronic structure methods use the law of quantum mechanics by solving the Schrodinger Equation:

$$H\Psi = E\Psi \tag{2.1}$$

where H is the Hamiltonian operator, E is the energy, and Ψ is the wave function that defines the quantum system.

Molecular mechanics calculations don't consider electrons (only based on interactions among nuclei), so it is inexpensive. But neglect of electrons makes it incapable to describe reactions which involve bond breaking and formation. Since we are interested in the reaction process, in this work, only electronic structure methods will be employed.

Usually there are three major classes of electronic structure methods: semi-empirical methods, such as AM1 and PM3; *ab initio* methods and density functional

methods (DFT). *Ab initio* and DFT methods will be used in this work. *Ab initio* methods construct the Hamiltonian and the wave function from first principles and an example is Hartree–Fock (HF) theory. In density functional theory, the wave function is approximated by a density functional and the energy is derived from the electron density. DFT methods include the effects of electron correlation and hence can provide the benefits of some more expensive *ab initio* methods at essentially HF cost.

The Hamiltonian operator can be written in the following form: $H = T + V$, and the general construction is shown in Equation 2.2:

$$H = -\sum_{i=1}^{N} \frac{\mathrm{h}^2}{2\mathrm{m_e}} \nabla_i^2 - \sum_{A=1}^{M} \frac{\mathrm{h}^2}{2\mathrm{M_A}} \nabla_A^2 - \sum_{i=1}^{N} \sum_{A=1}^{M} \frac{e^2 Z_A}{r_{iA}} + \sum_{B=1}^{M} \sum_{A=1}^{M} \frac{e^2 Z_A Z_B}{r_{AB}} + \sum_{i=1}^{N} \sum_{j>i}^{M} \frac{e^2}{r_{ij}} \qquad (2.2)$$

where h is Planck's constant divided by 2π; the constants m_e and M_A are the masses of the electron e and the nucleus A, respectively; e is the constant of elementary charge, and Z is the atomic number. This Hamiltonian can be presented in a more palpable form by setting the constants (i.e., m_e, e) to unity, which is shown in Equation 2.3:

$$H = -\sum_{i=1}^{N} \frac{\nabla_i^2}{2} - \sum_{A=1}^{M} \frac{\nabla_A^2}{2M_A} - \sum_{i=1}^{N} \sum_{A=1}^{M} \frac{1}{r_{iA}} + \sum_{B=1}^{M} \sum_{A=1}^{M} \frac{Z_A Z_B}{r_{AB}} + \sum_{i=1}^{N} \sum_{j>i}^{M} \frac{1}{r_{ij}} \qquad (2.3)$$

In this equation, the first two terms are the kinetic energy operators of the electrons and nuclei, respectively. The third term is the attractive potential between the electrons and the nucleus while the fourth term is the repulsive potential between the nuclei in a polyatomic system. Last is the term for the electron correlation energy, which is dependent on the distance between the *i*th and *j*th electrons (r_{ij}).

The nuclear and electronic motions are decoupled in the Born–Oppenheimer

approximation and the electronic energy is solved in an external potential from the fixed nuclei. With this approximation, the Hamiltonian can be rewritten as Equation 2.4:

$$H = -\sum_{i=1}^{N} \frac{\nabla_i^2}{2} - \sum_{i=1}^{N} \sum_{A=1}^{M} \frac{Z_A}{r_{iA}} + \sum_{i=1}^{N} \sum_{j>i}^{M} \frac{1}{r_{ij}} + V_{NN} \tag{2.4}$$

V_{NN} is an external potential at fixed nuclear coordinates.

1.2 Hartree-Fock Theory

The wave function Ψ, for some small systems (e.g. hydrogen atom), it is exact. However, for most polyatomic systems, Ψ is approximated. For normalized wave functions that satisfy the boundary conditions, the Variational Principle states that the variational energy (E_i) is an upper bound to the exact energy, E_0 (i.e. $E_i \geq E_0$). In Hartree-Fock (HF) theory, the spin orbitals are used as an approximate wave function and Equation 2.5 is derived by minimizing E_i with respect to the spin orbitals.

$$F_i \varphi_i = \varepsilon_i \varphi_i \tag{2.5}$$

In this equation F_i is the one electron Fock operator, φ_i are the HF molecular orbitals (MOs), and ε_i are the HF orbital energies. Fock operator F_i and φ_i can be expressed in Equations 2.6 and 2.7:

$$F_i = h_i + \sum_{i}^{N} (2J_i - K_i) \tag{2.6}$$

$$\varphi = \sum_{i=1} c_{is} \phi_s \tag{2.7}$$

where h_i is comprised of the electron kinetic and electron–nuclear potential energy terms.

The repulsive force between the *i*th and *j*th electrons is expressed by the 2e Coulomb integral, J_{ij}, and represents a net destabilization of the energy. The exchange between electrons in these spin orbitals is expressed by the 2e Exchange integral, K_{ij}, and results in a stabilization of the energy.

In HF theory, the MOs are linear combination of atomic orbitals (LCAO), which is used to approximate the wave function, see Equation 2.7. The set of functions used is called a basis set. The basis set can be interpreted as restricting each e to a particular region of space. Large basis sets impose fewer constraints on electrons and more accurate molecular obitals.

Also, the wave function must obey the Pauli Principle which states that the wave function must be anti-symmetric with respect to a change in the spatial location or spin of an electron. Slater proposed an approximate form for the wave function that obeys the Pauli Principle by representing it as a determinant, which is known as Slater Determinant.

1.3 Density Functional Theory

The HF theory does not consider electron correlation and there have been a variety of "post SCF" (Self-Consistent Field) solutions that have been proposed to correct the HF energy (i.e., perturbation theory, coupled-cluster theory, configuration interaction, etc.). In density functional theory (DFT), the energy of a system is determined from the electron density $\rho(r)$ of the system. The time-independent Schrodinger Equation is written as:

$$H\Psi = E_{\mathrm{DFT}[\rho]}\Psi \tag{2.8}$$

and the $E_{\mathrm{DFT}[\rho]}$ is:

$$E_{\mathrm{DFT}[\rho]} = T_{\mathrm{ni}}[\rho(\mathrm{r})] + V_{\mathrm{ne}}[\rho(\mathrm{r})] + V_{\mathrm{ee}}[\rho(\mathrm{r})] + \Delta T[\rho(\mathrm{r})] + \Delta V_{\mathrm{ee}}[\rho(\mathrm{r})] \tag{2.9}$$

where T_{ni}, V_{ne}, and V_{ee} are the electron kinetic, electron-nuclear potential, electron–electron energies, respectively. ΔT and ΔV_{ee} are the corrections to the kinetic and electron-electron energies, respectively.

The ΔT and ΔV_{ee} terms are the exchange-correlation energy, which is unknown and has been the primary focus of DFT development. A popular density functional that approximates the exchange and correlation energies is B3LYP, which is a combination of the Becke3 (B3) exchange[12] and Lee–Yang–Parr (LYP) correlation[13] functions, respectively.

In the last several years, the computational quantum chemistry methods have been developed in a way that allows estimations of thermodynamic properties for gas-phase species. Based on the quantum chemistry theory, the Gaussian series of computational chemistry programs were developed to predict many properties of molecules and reactions.[14] Computations can be carried out on systems in the gas phase or in solution, and in their ground state or in an excited state. Gaussian can serve as a powerful tool to explore reaction energies and reaction mechanisms.

2. Experimental Analysis

There are a variety of experimental techniques to characterize and evaluate chemical reactivity, especially calorimetric measurements. Experiments provide a good

understanding of the energy content of a substance and its behavior under various conditions, which is extremely useful for risk management. Calorimeters can be operated under various principles. However, four major operating principles have been used in chemical reactivity evaluation procedure including isothermal, isoperibolic, adiabatic, and temperature-programmed calorimeters. A comparison of these calorimetric operation principles is discussed extensively in the literature.[15]

Usually, reactive system screening tool (RSST) or differential scanning calorimeter (DSC) are used for preliminary analysis and automated pressure tracking adiabatic calorimeter (APTAC) is used for a more detailed characterization of the temperature and pressure profiles of the reaction. The vent sizing package (VSP) can provide information of scale-up.

The experimental results of these calorimeters vary based on the operating mode, sample size, precision, and sensitivity. Comparisons of the various calorimetric methods are available in the Center for Chemical Process Safety (CCPS) book.[16] In this work, DSC and APTAC are performed to obtain both the amount of energy released and the rate of energy released for a specific reactive chemical.

2.1 DSC

DSC is a popular screening tool (safe and fast) and can provide an overall indication of exothermic activity of the chemical being tested. In a DSC, a sample and a reference are subjected to a continuously increasing temperature and heat is added to the reference to maintain it at the same temperature as the sample. This added heat

compensates for the heat lost or gained as a consequence of an overall endothermic or exothermic reaction. When the rate of heat generation in the sample exceeds a particular value, the heat supply to the sample is cut off and this additional heat gain is attributed to exothermic activity within the sample.[17]

From the DSC data, onset temperature and heat of reaction can be determined. The onset temperature (T_o) is a measure of the reaction kinetics and serves as a guideline for selecting process or storage temperature. The energy released ($-\Delta H$) during the process is calculated as the area under the heat-supplied and time curve.

2.2 APTAC

Application of adiabatic thermal analysis techniques to evaluate reactive chemical hazards has motivated researchers to develop specifically designed adiabatic calorimeters for chemical reactivity hazards assessment. Following the screening tests, detailed measurements are generally performed for more hazardous chemicals using an adiabatic calorimeter such as APTAC. The APTAC minimizes the heat loss to the surrounding by maintaining the surrounding temperature as close to the sample temperature, and has proven to be an extremely useful tool to assess thermal hazards. Heldt and Anderson have discussed the application of modified adiabatic calorimeters to perform chemical reactivity analysis.[18]

The APTAC can be operated in a variety of test modes, such as heat-wait-search, heat-ramping, and isothermal. If the self-heat rate of the sample is greater than a preset threshold (0.1 ^{o}C/min), the apparatus tracks the reaction adiabatically until the reaction is

over or if one of the shutdown criteria is met. If no exotherm is detected, the sample is heated to the next search temperature and the steps are repeated until one of the shutdown criteria is met. Besides the temperature, the pressure outside the sample cell is controlled to match the pressure inside the sample cell.[19]

3. Conclusions

An evaluation of chemical reactivity depends on essential information, which includes process operating conditions, process chemistry, conditions under which chemical reactive hazards can appear. The huge number of reactive chemicals and a variety of operating conditions makes the dependence on experimental analysis alone quite expensive. The need to introduce a theoretical approach or combination of theoretical and experimental methods is necessary. This approach is a combination of theoretical and experimental levels of evaluation to identify reaction mechanisms and estimate thermodynamic and kinetic parameters of potentially hazardous reactions.

CHAPTER III

CHEMICAL REACTIVITY OF METHYLCYCLOPENTADIENE *

1. Background

Methylcyclopentadiene (MCP), C_6H_8, has recently been involved in a serious industrial incident which occurred on December 19, 2007, in Florida.[20] The explosion destroyed a T2 laboratory and led to four fatalities and multiple injuries. T2 Laboratories were making methylcyclopentadienyl manganese tricarbonyl (MMT). MMT is an additive used to boost gasoline octane rating and is marketed as Ecotane by T2 Laboratories and is sold in about 70 nations.

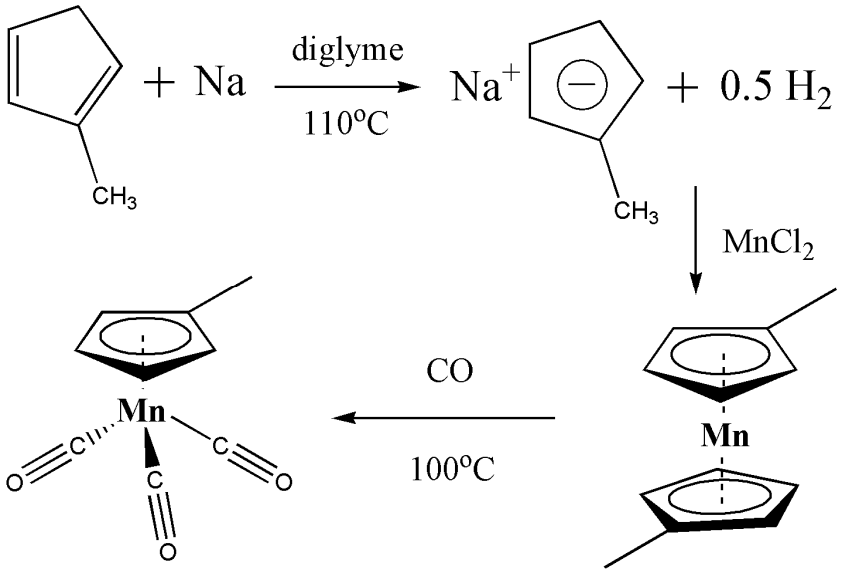

Figure 3.1. Summary of the process chemistry of manufacturing MMT.

---

* This chapter contains material reprinted with permission from Elsevier. Wang, Q.; Zhang, Y.; Rogers, W. J.; Mannan M. S. Molecular Simulation Studies on Chemical Reactivity of Methylcyclopentadiene. *J. Hazard. Mater.* **2009**, *165*, 141-147.

The process chemistry of manufacturing MMT is summarized in Figure 3.1 from a U.S. patent.[21] Among the chemical process, the first step is carried out at 110 ºC in diglyme, which is a common solvent in organic synthesis. This reaction is considered to be very hazardous in a batch reactor process, because more than half a ton of metallic sodium reacts with MCP, and release hydrogen gas as a byproduct. Preliminary findings conducted by CSB indicate that large amounts of thermal energies led to a runaway reaction and caused a high-pressure reactor vessel to rupture.

It is well known that chemical reactivity information can be obtained from literature sources or by using calorimetric techniques in the laboratory. However, for reactive materials with insufficient experimental data, such as MCP, estimation methods are of prime importance. Molecular simulation has been used to provide a unique and reliable approach for prediction of reactive hazards, such as hydroxylamine, NH_2OH.[22] MCP is an example of a highly reactive, hazardous, and poorly characterized compound in industry. It is reported that MCP is usually stored below -20 ºC, or in very diluted alcoholic solution. Dimerization is measurable above 0 ºC and normally completes within 2-3 hours at 60 ºC.[23] Since MCP is not commercially available (only methylcyclopentadiene dimer 93% can be purchased from Sigma–Aldrich Co.), the experimental evaluation of its calorimetric data is extremely difficult.

Reaction pathways, thermodynamic properties and kinetic parameters are important parts of chemical reactivity characterization. Hazardous reactions of MCP include ring expansion, decomposition, isomerization, dimerization, polymerization and oxidation. The pyrolysis of MCP has been examined in two shock tubes with a variety of

techniques by Ikeda et al.[24] High temperature shock tube results on the decomposition demonstrated that a large number of higher aromatics were produced. Five-member ring expansion in MCP is a transition from aliphatic to aromatic compounds, which has been theoretically investigated by Dubnikova et al.[25]

In this chapter, the chemical reactivity, especially the heat of reaction and isomerization, dimerization and oxidation reactions of MCP was thoroughly analyzed using the molecular simulation approach. The theoretical computational methods were used to predict plausible hazardous reaction pathways and their heats of reactions. Identification of the dominant reaction pathways will lead to a better understanding of the thermodynamic and kinetic characterization of MCP.

2. Theoretical Methods

Density functional and *ab initio* computations for the gaseous phase at 298 K and 1 atm were performed using the Gaussian-03 program package. A variety of theoretical methods, Austin Model 1 (AM1), Hartree-Fock (HF), Second-Order Møller-Plesset perturbation theory (MP2) and Becke 3 Lee, Yang, and Parr density functional theory (B3LYP) were used for geometry optimizations and frequency calculations. Employed also were Pople-style basis sets[26], 6-31G(d), including polarization functions for angular flexibility to represent regions of high electron density among bonded atoms.

One way to calculate enthalpies of reaction is to calculate heats of formation, and take the appropriate sums and difference. However, the heat of reactions can be obtained also by simply taking the difference of the sum of these values for the reactants and the

products, because the Gaussian program provides the sum of electronic and thermal enthalpies.[10] The same method can be used to calculate Gibbs free energies of reactions.

Frequency calculations at several levels of theory were performed to obtain zero-point energies and frequencies for all species in the reaction pathways without symmetry restrictions. Each calculated structure was characterized as either a local minimum with no imaginary frequency or a transition state with only one imaginary frequency. Vibrational analysis was also at the same level of theory to characterize the optimized structures as local minima or transition states**.** The QST2 method was used to search and optimize the transition state structures. The calculation of intrinsic reaction path (IRC) was also conducted to follow the reaction pathways and used to check whether a transition state connects two minima of interest on the potential energy surface.

3. Results and Discussion

3.1 Isomerization Reaction

As a product of thermal cracking of petroleum hydrocarbons, MCP has three isomers depending upon the location of the methyl group with respect to the SP^3 carbon in the molecule (Figure 3.2). All three isomers are optimized using AM1, HF, MP2, and B3LYP, with the same basis set, 6-31G(d). All of the total energies and relative energies including the zero-point energy (ZPE) correction are summarized in Table 3.1. As can be seen, these theoretical methods give the consistent results that the lowest energy isomer is 2-MCP.

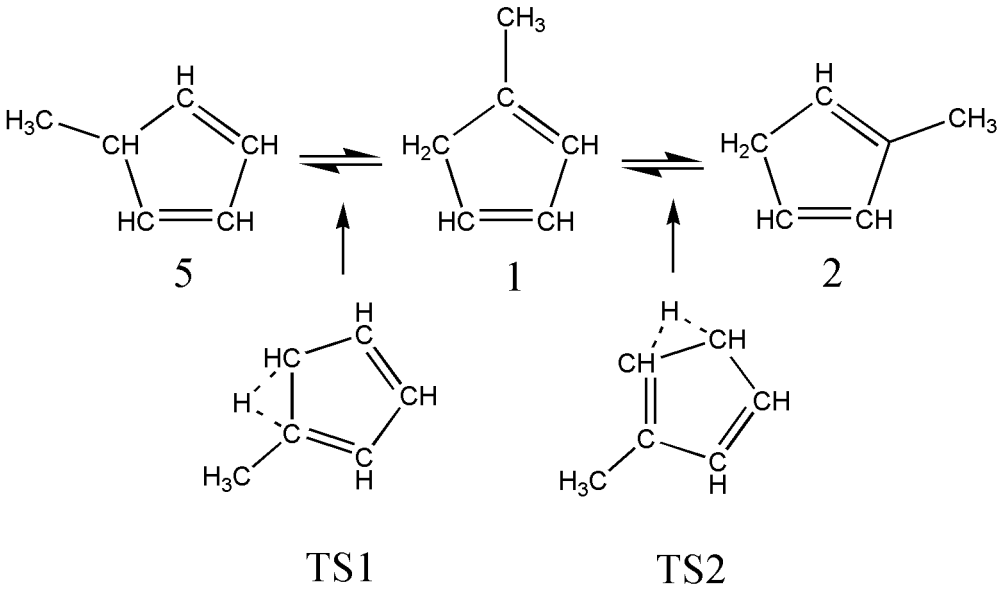

Figure 3.2. Isomerization mechanism of three MCP isomers.

Table 3.1. Total energies and relative energies including zero-point energy (ZPE) correction of three isomers.

Isomers	**HF**		**MP2**		**B3LYP**		**AM1**	
	E	Δ*E*	*E*	Δ*E*	*E*	Δ*E*	*E*	Δ*E*
2	-231.7137	0.00	-231.7135	0.00	-233.3030	0.00	0.1680	0.00
1	-231.7134	0.25	-231.7131	0.26	-233.3028	0.15	0.1684	0.24
5	-231.7077	3.78	-231.7073	3.91	-233.2958	4.51	0.1755	4.46

The mechanisms of sigmatropic rearrangements have been systematized by the Woodward-Hoffmann rules of orbital symmetry, and concerning the nature of the [1,5] rearrangement also has been reported by Spangler.[27] Particularly, the [1,5] sigmatropic hydrogen shifts in the heterocycles have been examined using *ab initio* calculations.[28] It would be interesting to know the isomerization mechanism and rates in the three isomers of MCP. In this case, the isomerization reactions from 2-MCP to 1-MCP, and also from 1-MCP to 5-MCP can be described in a sigmatropic [1,5] hydrogen shift mechanism, as shown in Figure 3.2. The reaction coordinate involves a substantial H-atom motion as the carbon-carbon double bonds rearrange.

A transition state is defined as the geometry that has a zero derivative of energy and a positive second derivative of energy with respect to movement of the nuclear coordinates for all but one geometric movement, which has a negative curvature. The energy of the transition state structure must be calculated to determine the activation energy and the reaction rate.

In this chapter, we use the QST2 method to calculate the configuration and the energies of the transition states of two isomerization reactions. The transition structures, TS1 and TS2 as shown in Figure 3.2, are obtained and each have only one imaginary frequency (-1227.29 cm^{-1} for TS1, -1263.93 cm^{-1} for TS2). The energy barrier of the 2-MCP to 1-MCP isomerization is 27.98 kcal/mol at the B3LYP level of the theory, whereas the barrier for isomerization of 1-MCP to 5-MCP is 24.05 kcal/mol. The activation energy difference can be explained by the relatively small endothermicity of the 2-MCP to 1-MCP isomerization compared to the 1-MCP to 5-MCP isomerization.

The values of activation energy are consistent with the experimental results reported by McLean et al.[29] Therefore, the reaction rate constant *k* can be estimated based on Transition State Theory (TST).

TST can be derived from chemical quasi-equilibrium between reactants and transition states. It can be used to explain the reaction rates of elementary chemical reactions. For the quasi-equilibrium assumption, it is different from classical chemical equilibrium. Consider the reaction below:

$$A + B \leftrightarrow [AB]^{\ddagger} \rightarrow P \tag{3.1}$$

where complete equilibrium is achieved between all the species in the system including activated complexes, $[AB]^{\ddagger}$. The equilibrium constant $K^{\ddagger\Theta}$ for the quasi-equilibrium can be written as

$$K^{\ddagger\ominus} = \frac{[AB]^{\ddagger}}{[A][B]} \tag{3.2}$$

Therefore, the concentration of the transition state $[AB]^{\ddagger}$ can be expressed as

$$[AB]^{\ddagger} = K^{\ddagger\Theta}\,[A]\,[B] \tag{3.3}$$

From the rate equation, the concentration of the product P is

$$\frac{d[P]}{dt} = k^{\ddagger\ominus}[\mathrm{AB}]^{\ddagger} = k^{\ddagger}K^{\ddagger}[A][B] = k[A][B] \tag{3.4}$$

$k^{\ddagger}$ is directly proportional to the frequency of the vibrational mode (ν) responsible for converting the activated complex to the product. Every vibration does not necessarily lead to the formation of product, so a proportionality constant κ, referred to as the transmission coefficient, is introduced to account for this effect. Hence, $k^{\ddagger}$ can be rewritten as

$$k^{\ddagger} = \kappa\nu \tag{3.5}$$

For the equilibrium constant $K^{\ddagger}$, statistical mechanics leads to a temperature dependent expression given as

$$K^{\ddagger} = \frac{k_B T}{h\nu} K^{\ddagger'} \tag{3.6}$$

where

$$K^{\ddagger'} = e^{\frac{-\Delta G^{\ddagger}}{RT}} \tag{3.7}$$

Combining the new expressions for $k^{\ddagger}$ and $K^{\ddagger}$, the rate constant expression can be written as

$$k = k^{\ddagger} K^{\ddagger} = \kappa \frac{k_B T}{h} e^{\frac{-\Delta G^{\ddagger}}{RT}} \tag{3.8}$$

Since $\Delta G = \Delta H - T\Delta S$, the rate constant expression can be expanded to

$$k = \kappa \frac{k_B T}{h} e^{\frac{\Delta S^{\ddagger}}{R}} e^{\frac{-\Delta H^{\ddagger}}{RT}} \tag{3.9}$$

where k_B is Boltzmann's factor, h is Planck's constant, T is the absolute temperature and R is the gas constant. Both $k_{5\text{-}1}$ and $k_{1\text{-}2}$ are estimated to be 1.42×10^{-5} s^{-1}, 1.86×10^{-8} s^{-1}, respectively, at 298 K and 1 atm from molecular modeling.

As described before, the equilibrium constant $K^{\ddagger}$ is defined by the relation:

$$K^{\ddagger'} = e^{\frac{-\Delta G^{\ddagger}}{RT}} \tag{3.10}$$

When the reaction system reaches equilibrium, $K^{\ddagger}$ can be calculated according to equation (3.10) for the chemical equilibrium among the three isomers. Therefore, the molar ratio (or ratio of concentration) of three isomers can be estimated to be 0.61:0.39:0.0006, for 2-MCP, 1-MCP, 5-MCP respectively, at 298 K and 1 atm.

3.2 Dimerization Reaction

From the results of section 3.1, because more than 60% of isomers are 2-MCP under the chemical equilibrium condition, 2-MCP is selected as the starting material in the following reactions. Dimerizations of 2-MCP follows the Diels–Alder reaction, which has been studied in great detail both theoretically and experimentally.

Three possible mechanisms have been proposed by Woodward for the Diels–Alder reactions: a concerted mechanism, a two-step mechanism, and an asynchronous two-stage mechanism.[30] The concerted mechanism suggests that the reactants will dimerize directly to the final product through an activated transition state barrier. However, the two-step mechanism suggests the formation of various diradicals as the first step followed by the formation of the product as the final step. The asynchronous two-stage mechanism is a combination of the two previous mechanisms.

Several semi-empirical and *ab initio* theoretical studies of Diels–Alder cycloadditions have been conducted: some studies have shown that *ab initio* SCF methods favor a concerted mechanism, while semiempirical approaches favor steps involving biradicals. Diels–Alder dimerizations of a series of substituted cyclopentadienes have been studied by Froese et al,[31] but the dimerization reaction has not been investigated.

In this work, the two-step mechanism is proposed, as shown in Figure 3.3. There are twelve reactions with three different reaction pathways and twelve final products. To determine the dominant reaction pathways and their thermo-kinetic parameters, computational quantum chemistry calculations were performed using three different

levels of theory. The resulting heats of reaction and Gibbs free energies are summarized in Table 3.2.

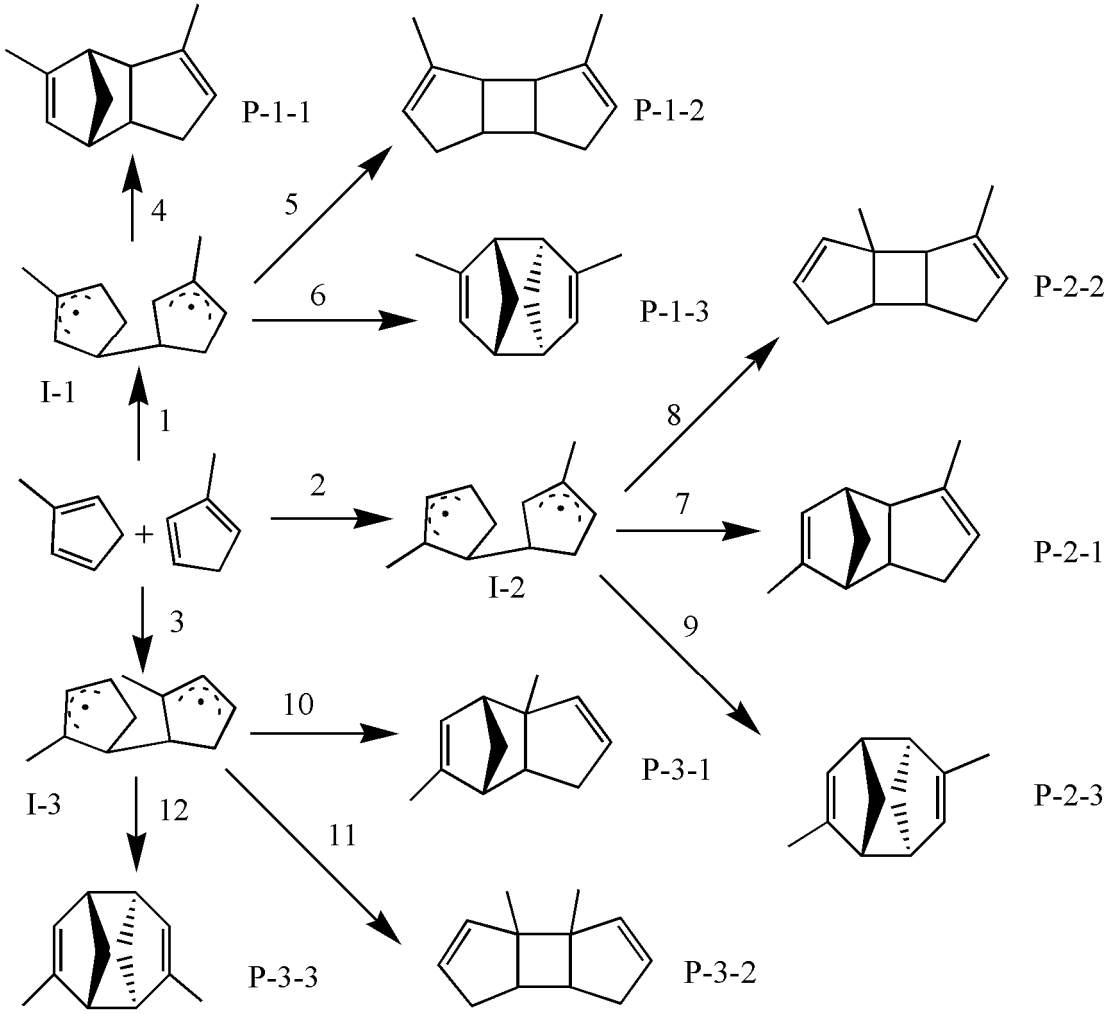

Figure 3.3. A two-step mechanism of dimerization reactions.

Table 3.2. Heats of reactions (ΔH_r) and Gibbs free energies (ΔG_r) of dimerization reactions of 2-MCP calculated using three levels of theory.

Reactions	**AM1**		**HF**		**B3LYP**	
	ΔH_r	ΔG_r	ΔH_r	ΔG_r	ΔH_r	ΔG_r
1	-14.26	-4.08	-4.37	4.56	-2.36	2.25
2	-14.17	-2.32	-4.34	5.69	-3.12	2.38
3	-13.09	0.61	-3.03	8.07	2.71	5.48
4	-4.75	-0.91	-9.57	-6.29	-10.40	-2.32
5	34.29	39.54	-0.39	5.52	-2.10	2.97
6	7.61	14.10	14.24	21.33	9.90	16.31
7	-4.84	-0.81	-9.33	-7.14	-9.29	-4.41
8	38.28	42.02	0.84	8.77	-0.35	5.38
9	7.58	12.39	11.56	16.56	9.61	15.10
10	1.32	3.99	-6.30	0.94	-4.63	2.38
11	50.57	53.79	45.62	50.37	35.29	43.18
12	6.44	9.41	12.90	17.82	18.67	23.63

To simplify the procedure of predicting the kinetics of elementary reactions, a linear thermodynamic–energy correlation, the Evans–Polanyi Equation,[32] is commonly used to estimate activation barriers from heats of reactions:

$$E_a = E_a^0 + \gamma_P \Delta H_r \tag{3.11}$$

where E_a^0 is the intrinsic activation barrier, γ_P is the positive transfer coefficient, and ΔH_r is the heat of reaction. This equation indicates that as a reaction type becomes more exothermic, its activation barrier decreases. Hence, it is possible to apply Equation 3.11 to identify the dominant pathways based on activation energy predictions of proposed elementary reactions.

Since reactions 1, 2, and 3 share the same mechanism, E_a^0 and γ_P values are expected to be the same for the three reactions. All three theoretical methods (AM1, HF and B3LYP) give the same results which are sufficient to conclude that reactions 1 and 2 are dominant over 3 since they have the lower heats of reaction. Therefore, diradicals I-1 and I-2 will be the main intermediates. Similarly, reactions 4 5, and 6 proceed with the same mechanism, however, reaction 4 has much lower heat of reaction (-10.4 kcal/mol) than reaction 5 and 6 (-2.1 kcal/mol and 9.9 kcal/mol, respectively), which is expected to have lower activation barrier and therefore is more dominant. Also, among reactions 7, 8 and 9, reaction 7 is expected to be more dominant.

On the basis of this analysis, the main dimerization reaction pathways are through intermediate I-1 and I-2, to form product P-1-1 (dimerization 1) and P-2-1 (dimerization 2). The optimized molecular structures of these main final products are shown in Figure 3.4. Previous experiment using a gas chromatograph to separate the

mixture of dimers indicated that P-1-1 and P-2-1 are the major compositions, which is consistent with the simulation result.[33] As for the overall heats of reactions, B3LYP level calculations yield -12.75 kcal/mol and -12.41 kcal/mol, for dimerization 1 and dimerization 2, respectively.

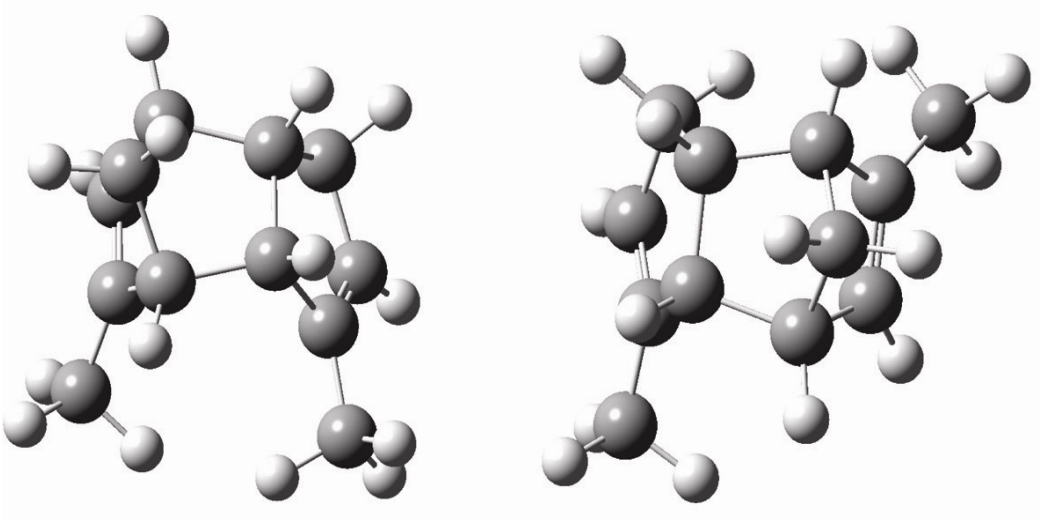

Figure 3.4. Molecular structures of two major products in dimerization reactions.

3.3 Oxidation Reaction

Singlet ($^1\Delta_g$) oxygen addition to unsaturated and aromatic compounds, which involves the formation of organic peroxides and hydroperoxides, plays an important role in chemical processes, which can directly initiate a chain of radical reactions. 1,4-cycloaddition of oxygen to a system containing two conjugated double bonds results in the formation of the 1,4-peroxides. Two different mechanisms were suggested for 1,4-oxygen addition: a stepwise mechanism involving a linear biradical intermediate, and a

single-step mechanism with a symmetric transition structure with significant charge transfer from the organic donor to oxygen. The first mechanism involving linear biradical intermediates seems to be reasonable. Although there is no direct experimental evidence to support this mechanism, it is possible, because the intermediates have been observed in the reaction of singlet oxygen with 2,4-hexadiene.

In this chapter, possible reaction pathways are suggested based on the first mechanism and are illustrated in Fig. 3.5. The reactions will lead to the formation of highly reactive peroxide, which may initiate the polymerization of MCP. The quantum computational level of theory was used to predict the reaction thermodynamic values presented in Table 3.3.

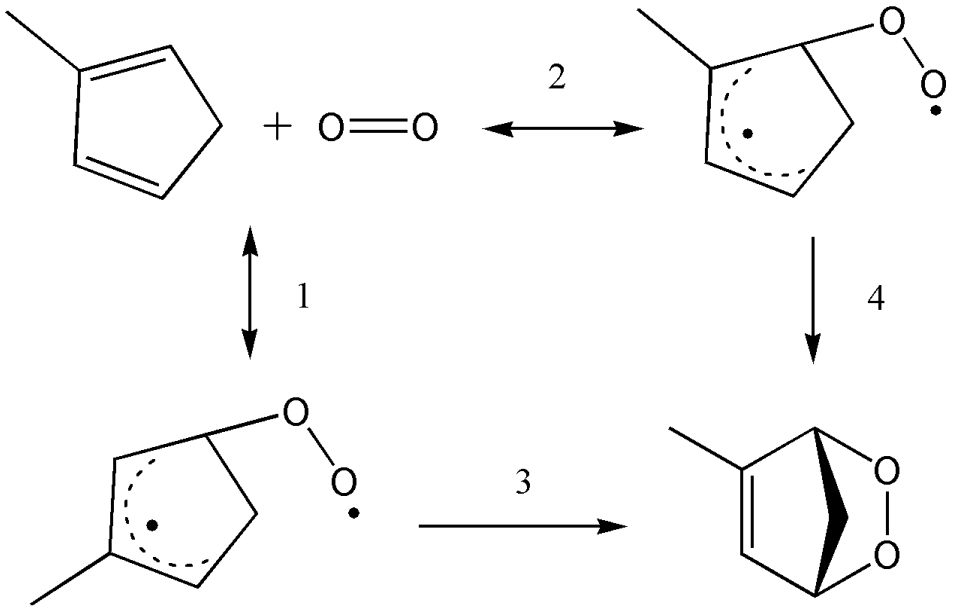

Figure 3.5. Proposed reaction pathways of oxidation reactions.

Table 3.3. Heats of reactions (ΔH_r) and Gibbs free energies (ΔG_r) of oxidation reactions of 2-MCP calculated using three levels of theory.

Reactions	**HF**		**MP2**		**B3LYP**	
	ΔH_r	ΔG_r	ΔH_r	ΔG_r	ΔH_r	ΔG_r
1	-41.82	-32.93	-11.54	-8.58	-23.47	-14.25
2	-41.79	-33.84	-10.92	-7.95	-22.70	-13.75
3	-0.32	3.33	-33.67	-24.07	-25.98	-22.76
4	-0.35	4.24	-34.30	-24.70	-26.75	-23.25

According to the results of the calculations, the oxidation reaction is significantly exothermic. The reaction involves the formation of intermediates, in which the oxygen molecule is attached to one of the terminal carbon atoms. Applying the same concepts of reaction pathway predictions on reactions with oxygen as in Figure 3.5 suggests that the organic peroxide will be formed.

Compared to dimerization reactions, it is found that the peroxide formation reactions generally have lower activation barriers (higher heat of reaction is released) and hence may be dominant. Heat of these peroxide reactions is calculated to be -45.57 kcal/mol using the B3LYP level theory. The reactivity hazard of MCP is predicted to be more significant in the presence of air or any other free radical initiator, because the energy release associated with the oxidation reactions exceeds those of the dimerization reactions.

3.4 Investigation of T2 Laboratories Explosion

As it was mentioned by the U.S. Chemical Safety Board (CSB) in its investigation on the T2 Laboratories explosion, excessive reactor pressure and temperature led to a runaway chemical reaction and an explosion. Part of the reactor vessel ruptured and injuries occurred 750 feet from the reactor's location with debris found a mile from the blast. The CSB team may conduct reactive chemistry testing to analyze the chemical hazards leading to the reactor failure. But this testing and analysis could take more than a year to result in a published review.

Molecular simulation, however, is a quick and reliable approach to estimate this incident. Here, the available information was used to find the possible causes and reduce the likelihood of such accidents. Based on the process chemistry analysis and a molecular simulation approach, some potential causes of the T2 Laboratories explosion incident are identified as follows:

1. The first step of the chemical process includes the mixing of reactive materials (MCP) with metallic sodium and generates hydrogen gas, which will cause a pressure increase in the reactor. Hydrogen gas is very easy to be ignited because of its low minimum ignition energy, a high flame speed, and a wide range of flammability. Also vapors from MCP can ignite at 80 ºC according to safety warnings for the chemical solution.

2. MCP is highly reactive and will dimerize even at 0 ºC as mentioned previously. From the molecular simulation results, the dimerization reaction is thermodynamic feasible and exothermic ($\Delta H_r \approx$ -15 kcal/mol) at 298 K and 1 atm. Exothermic reactions generate heat, which causes the temperature in the vessel to rise. If the thermal energy is not efficiently dissipated to the surroundings, it will finally lead to an unexpected runaway reaction.

3. Molecular simulation results also indicate that the oxidation reaction is more favorable than dimerization reactions in the presence of air. Large amounts of reaction heat ($\Delta H_r \approx$ -46 kcal/mol) will be released, and peroxide intermediates will be produced. The peroxides will increase the chance of polymerization reaction initiation and therefore increase the reactivity hazards.

The molecular simulation approach could provide some guidance for the safer chemical processes and safer handling of MCP. For example, since both dimerization reactions and oxidation reactions are quite exothermic, it is especially important to control the local temperature and pressure inside the reactor for the reactions with MCP involved, and efficiently dissipated the thermal energies to the surroundings. Organic peroxides, which can be produced by oxidation reactions, will also initiate polymerization reactions. Therefore, MCP should be handled or fed to the reactor very carefully under nitrogen atmosphere. Another concern is the possibility of changing the chemical process.

Roesky et al. reported an improved synthesis of sodium cyclopentadienide directly by the reaction of dicyclopentadiene with metallic sodium.[34] From the molecular simulation results, the dimers of MCP are much more stable than its monomers. Therefore, it might explore the dimers as the starting material and synthesize MCP, which will be used *in situ* for the next reaction.

4. Conclusions

Molecular simulations were performed to investigate the chemical reactivity of MCP. It is possible to predict qualitatively the dominant reaction pathways of dimerization and oxidation through the application of quantum chemistry calculations and thermodynamic–energy correlation. Both the dimerization and oxidation reactions are quite exothermic. However, exposure of MCP to air is extremely dangerous due to the relatively high value of the oxidation reaction heat. Theoretical methods provide an understanding of reactive hazards at the molecular level and also guide strategies for safer handling of hazardous materials such as MCP. The results reported here could provide the support to the investigation of the T2 Laboratories explosion on December 19, 2007 in Florida.

CHAPTER IV

THERMAL DECOMPOSITION OF HYDROXYLAMINE *

1. Background

Hydroxylamine plays an important role in the semiconductor, chemical, and pharmaceutical industries. It is used as a solvent in microchip production to remove organic and inorganic impurities from wafers, and also as an important feedstock for dyes, rust inhibitors, and products, such as painkillers, antibiotics, and tranquillizers.[35] However, it is challenging to handle hydroxylamine free base, and nominally pure hydroxylamine is known to decompose at room temperature.[36] Its chemical instability has led to two tragic incidents in the industry.[37, 38]

Since then, thermal decomposition hazards of hydroxylamine/water solutions have been investigated using calorimeters.[39-44] Hydroxylamine decomposition has been found to be sensitive to metals,[44] metal ions,[40, 42] and pH of the solutions.[39] The final decomposition products were analyzed as NH_3, H_2O, N_2, N_2O, and small amount of NO and H_2, and the proportion of the products depends on experimental conditions.[41, 45]

$$2NH_2OH \longrightarrow H_2O + NH_3 + HNO \qquad (4.1)$$

---

* This chapter contains material which has been submitted to *Journal of Physical Chemistry A*. Wang, Q.; Wei, C.; Pérez, L. M.; Rogers, W. J.; Hall, M. B.; Mannan, M. S. Thermal Decomposition Pathways of Hydroxylamine: Theoretical Investigation on the Initial Steps. **2010**.

Previous experimental tests have provided only the overall decomposition behavior of hydroxylamine. The decomposition mechanism of hydroxylamine is still poorly understood, and the proposed mechanisms in the literature are controversial. Nitroxyl (HNO) was proposed to be an intermediate for the decomposition of hydroxylamine by Nast,[46] and a reaction (Equation 4.1) was developed in which the decomposition is controlled by disproportionation of hydroxylamine to water, ammonia, and nitroxyl. The presence of nitroxyl as an intermediate was verified by the appearance of the violet tricyanonitrosonickel(II) on the addition of tetracyanonickel(II).[46]

However, Lunak[47] disagreed with the conclusion and demonstrated that the formation of tricyanonitrosonickel(II) was not due to nitroxyl, but a tricyano-hydroxylammonium nickel complex, resulting from replacement of a cyanide group in tetracyanonickel (II) by a molecule of hydroxylamine. Holzapfel[48] studied the kinetics of hydroxylamine decomposition in strong alkaline solutions, and it was assumed that OH–NH–OH and OH–NH–NH–OH were formed during the decomposition.

In a previous study, it was found that acid or base can initiate different decomposition pathways of hydroxylamine.[39] Hughes[49, 50] reported the oxidation of hydroxylamine in alkaline solutions, and nitrite, peroxonitrite, and hydrogen peroxide were detected as intermediates in significant quantities together with some nitrate. Furthermore, the catalytic effects of metal ions on the decomposition of hydroxylamine were studied under different conditions.[47, 50-52]

In this chapter, hydroxylamine decomposition pathways were investigated in gas-phase and in aqueous solutions. As part of our ongoing interest in evaluating chemical

reactivity of hydroxylamine, we sought to elucidate the initiation decomposition steps of hydroxylamine using quantum mechanical calculations. Several possible decomposition pathways were proposed, and the most favorable decomposition pathway was determined. Density functional theory (DFT) and *ab initio* wave function theory (WFT) were employed to yield a quantitative description of the thermal decomposition mechanism. The results will provide a better understanding of the stability of hydroxylamine and guidance on the design of effective inhibitors to control the decomposition behavior.

2. Computational Details

Density functional and *ab initio* calculations were performed using the Gaussian 03 suite of programs.[53] All the geometries of reactants, products, various intermediates, and transition states were fully optimized in gas-phase using several density functional methods. The Becke3-Lee-Yang-Parr (B3LYP)[54, 55] and modified Perdew-Wang 1-parameter model for kinetics (MPW1K)[56] were used with Dunning's correlation consistent polarized valence double zeta basis set (cc-pVDZ)[57] and Pople-style basis set[58] including diffuse[59] and polarization[60] functions (6-31+G(d,p)), respectively.

Previous theoretical work[61,62] shows that the MPW1K method can provide more accurate energy barriers than B3LYP with lower cost performance. The Becke88-Becke95 1-parameter model for kinetics (BB1K) is a new hybrid Hartree-Fock density functional model developed by Truhlar et al., and a previous theoretical study shows that BB1K can give excellent saddle point geometries and barrier heights.[63] To validate the

DFT methods and achieve more accurate energies, single point energies were calculated with coupled cluster singles and doubles with triples correction CCSD(T)[64] using a 6-311+G(3df,2p) basis set, based on the optimized geometries obtained from the Møller-Plesset second-order perturbation theory (MP2)[65] with the same basis set. A composite complete basis set (CBS-Q)[66] method was also employed to calculate the decomposition pathways of unimolecular reactions.

The basis sets used for geometry optimizations and energy calculations were implemented as follows:

$$\text{cc-pVDZ} \rightarrow \text{BSI}$$

$$\text{6-31+G(d,p)} \rightarrow \text{BSII}$$

$$\text{6-311+G(3df,2p)} \rightarrow \text{BSIII}$$

Frequency calculations at the B3LYP, MPW1K, and MP2 levels of theory were performed to obtain zero-point energies and frequencies for all species in the reaction pathways. The calculated structures were characterized as either a local minimum with no imaginary frequency or transition states with only one imaginary frequency. Some intrinsic reaction path (IRC) calculations[67, 68] were conducted to follow the reaction paths and validate that the transition states connect two minima of interest on the potential energy surface.

Solvent effects on the decomposition pathways were studied using both cluster methods and Conductor Polarizable Continuum Models (CPCM).[34] Single point energy

calculations using the optimized gas-phase geometry were conducted with the CPCM due to geometry optimization convergence problems. Relative energies are reported in kcal/mol. Representations of the reactants, products, intermediates, and transition states, shown in Figures 4.1-4.3, were created using the JIMP 2 software program.[35]

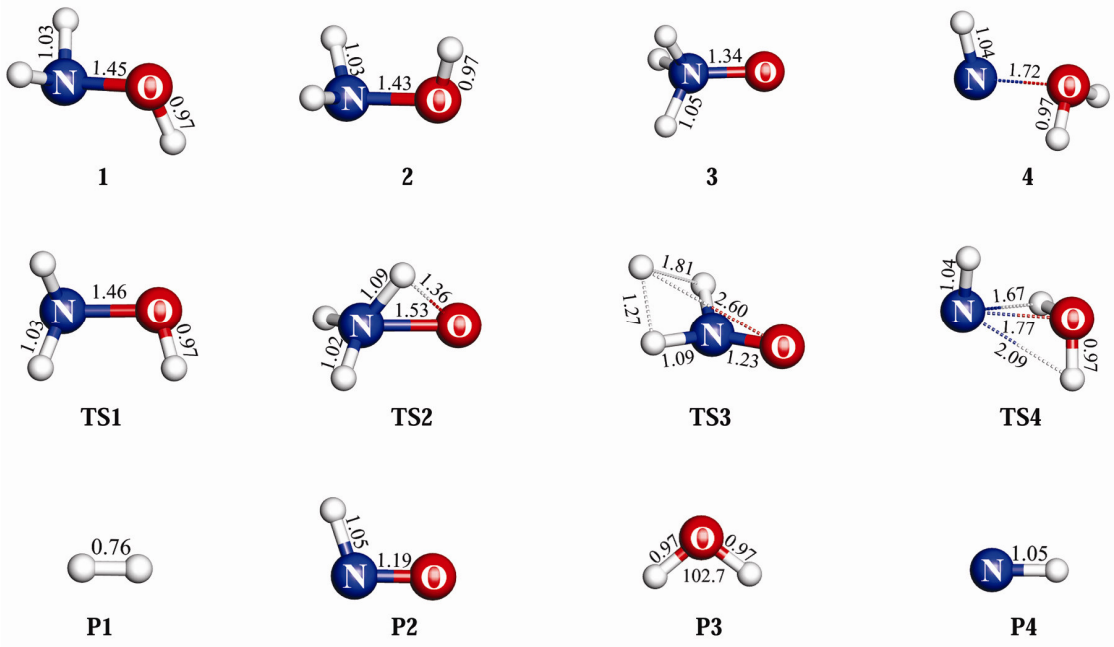

Figure 4.1. Molecular structures of hydroxylamine, transition states, and products involved in unimolecular decomposition pathways (pathways 1-4) at the level of B3LYP/BSI.[a]

[a] **P5** has the similar structure as **P4** with bond length 1.06 Å.

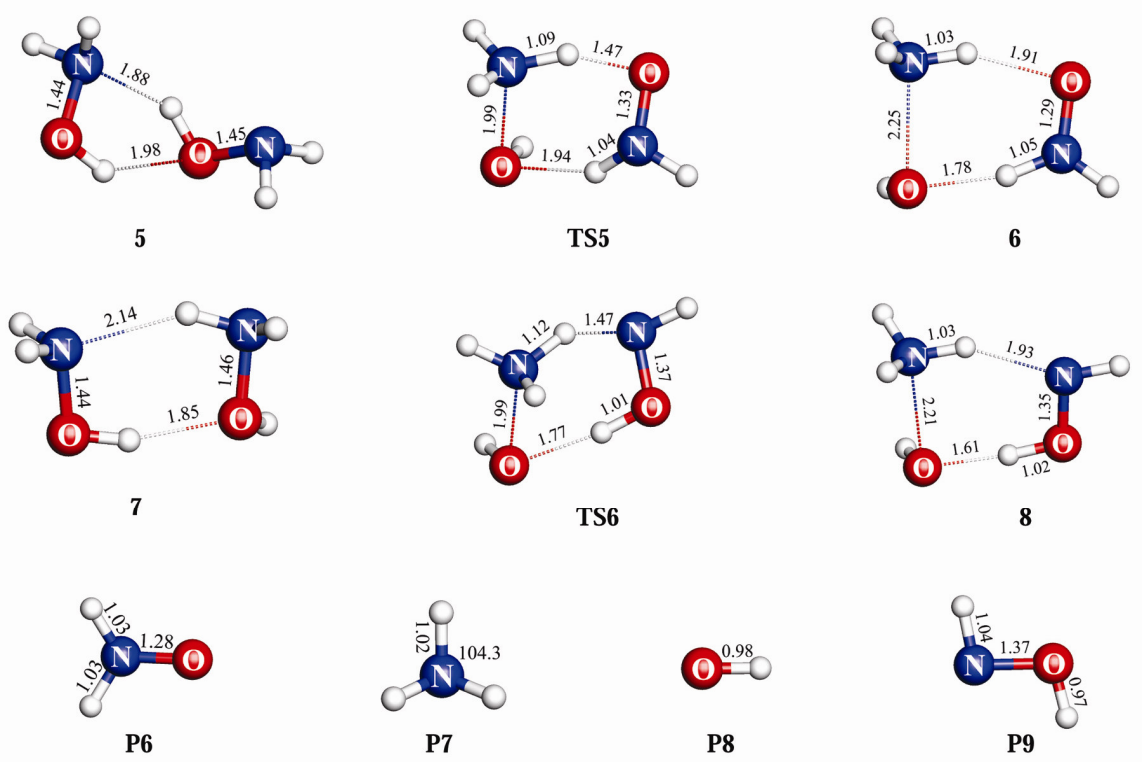

Figure 4.2. Molecular structures of hydroxylamine, transition states, and products involved in bimolecular decomposition pathways 5 and 6 at the level of B3LYP/BSI.

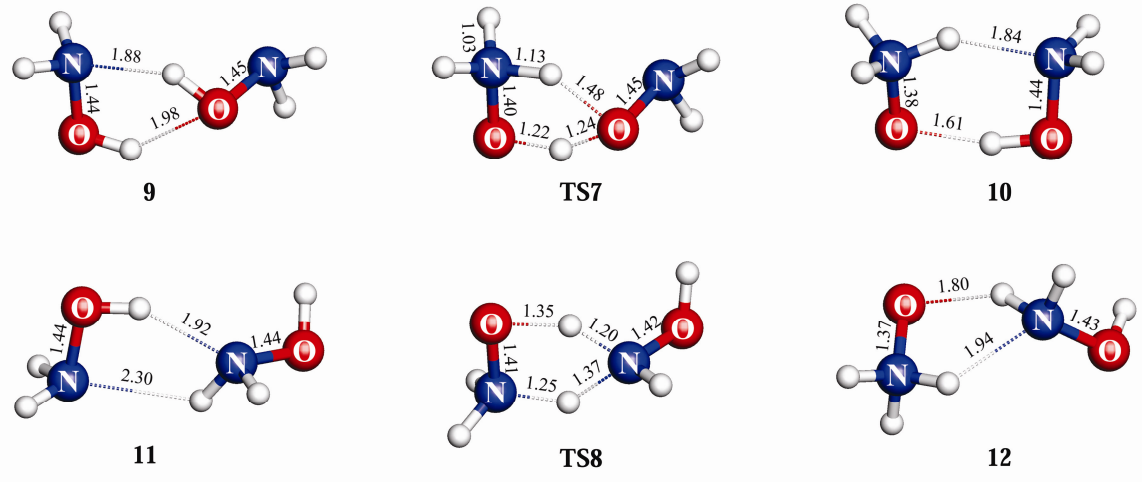

Figure 4.3. Molecular structures of hydroxylamine, transition states, and products involved in bimolecular decomposition pathways 7 and 8 at the level of B3LYP/BSI.

3. Results and Discussion

3.1 Molecular Structures of Hydroxylamine

Experimental data on the molecular geometry for hydroxylamine are available,[69] and some theoretical calculations[70, 71] on the heat of formation, equilibrium geometries, rotational barriers, and vibrational analysis have also been reported. Hydroxylamine (HA, **1**) is in C_s symmetry and has two conformations ("*trans*" and "*cis*"), as shown in Figure 4.1. The optimized geometries of **1** and **2** at the density functional and CCSD levels of theory are compared with experimental and previous theoretical results in Table 4.1.

B3LYP/BSI provides relatively accurate bond lengths within 0.01 Å of the experimental values, but a poor H–N–H bond angle (103.9º), compared with the experimental value (107.1º). MPW1K and BB1K results are very similar to each other, but the calculated N–O bond lengths are both 0.04 Å shorter than the experimental value, and the calculated H–N–H bond angles (106.8º and 106.6º, respectively) are closer to the experimental value (107.1º).

From the deviations in Table 4.1, CCSD/BSII provides slightly better results than MP2/BSIII, especially the bond lengths (zero deviation for CCSD/BSII compared with the experimental value). In order to obtain highly accurate results on the geometry of **1**, the CCSD level of theory with a relatively large basis set is necessary.

Table 4.1. Comparison of optimized geometries of NH_2OH at different levels of theory with experimental data (Bond lengths are in Å and Angles in ^{o}).

	Experi-mental[a]	B3LYP /BSI	MPW1K /BSII	BB1K /BSII	CCSD /BSII	MP2 /6-311++G(d,p)[b]	MP2 /BSIII[c]
trans-NH_2OH							
R_{N-H}	1.016	1.027	1.010	1.011	1.017	1.017	1.013
R_{N-O}	1.453	1.446	1.408	1.411	1.448	1.434	1.430
R_{O-H}	0.962	0.969	0.954	0.955	0.964	0.960	0.959
∠HNH	107.1	103.9	106.8	106.6	106.1	105.9	106.0
∠HNO	103.2	103.3	105.0	104.8	103.5	104.3	104.2
∠HON	101.4	101.7	103.7	103.6	102.4	101.8	102.4
cis-NH_2OH							
R_{N-H}		1.028	1.010	1.010	1.018	1.017	
R_{N-O}		1.428	1.397	1.400	1.436	1.423	
R_{O-H}		0.974	0.958	0.959	0.968	0.964	
∠HNH		105.7	109.2	109.1	108.0	107.9	
∠HNO		107.3	108.7	108.5	107.1	107.9	
∠HON		107.9	109.2	109.1	108.1	107.5	

[a] Tsunekawa, S. *J. Phys. Soc. Jpn.* **1972**, *33*, 167.
[b] Boulet P. et al., *Chem. Phys.* **1999**, *244*, 163.
[c] Chung-Phillips, A.; Jebber, K. A. *J. Chem. Phys.* **1995**, *102(18)*, 7080.

Table 4.2. Calculated relative energies, barrier heights ($\Delta^{\ddagger}E^{o}$ in kcal/mol), and optimized geometry of transition state between *trans* and *cis* conformation of NH_2OH (Bond lengths in Å and Angles in ^{o}).

Molecule	B3LYP /BSI[a]	MPW1K /BSII[a]	BB1K /BSII[a]	CCSD /BSII[a]	MP2 /BSII[b]	MP2 /BSIII[a]	CCSD(T)/BSIII //MP2/BSIII[a]
trans (**1**)	0.00	0.00	0.00	0.00	0.00	0.00	0.00
TS1	6.56	7.88	7.79	7.59	7.25	6.45	6.28
cis (**2**)	4.43	5.32	5.31	5.55	4.34	4.15	4.14
Geometry of **TS1**							
R_{N-H}	1.028	1.011	1.011	1.019	1.014	1.016	
$R_{N-H'}$	1.029	1.011	1.011	1.019	1.015	1.016	
R_{N-O}	1.457	1.421	1.424	1.461	1.444	1.448	
R_{O-H}	0.969	0.954	0.955	0.964	0.959	0.960	
∠HNH	102.7	105.6	105.5	105.1	104.4	104.3	
∠HNO	102.3	103.5	103.3	102.3	102.7	102.5	
∠H´NO	106.6	108.2	108.1	106.9	107.2	107.0	
∠HON	105.9	107.9	107.8	106.7	106.3	106.2	

[a] Zero-point energy (ZPE) included.
[b] Chung-Phillips, A.; Jebber, K. A. *J. Chem. Phys.* **1995**, *102(18)*, 7080.
[c] H and H´ are symmetry equivalent.

The rotational barrier for the conversion from *trans* conformation (**1**) to *cis* conformation (**2**) is not available from experiment but can be obtained from previously theoretical studies.[71, 72] The geometry of the transition state (**TS1**, see Figure 4.1) and the calculated rotational barriers at different levels of theory are presented in Table 4.2.

In previous work, it was shown that the calculated rotation barrier and energy of reaction decrease with the increase of the size of the basis sets and the correlation corrections.[71] In our work, the most accurate energies were obtained at the CCSD(T)/BSIII level of theory with the inclusion of zero point energy corrections at the MP2/BSIII level. The *trans* conformation is found to be 4.14 kcal/mol more stable than *cis* conformation, and the *trans* to *cis* rotation barrier at the CCSD(T)/BSIII//MP2/BSIII level is 6.28 kcal/mol.

The density functional theories with small basis sets provide higher barriers, especially MPW1K (7.88 kcal/mol) and BB1K (7.79 kcal/mol). Because the results from the MPW1K and BB1K calculations are so close, only MPW1K was employed for the pathway analysis. The rotation barrier and relative energy at the B3LYP/BSI level (6.56 kcal/mol and 4.43 kcal/mol, respectively) are close to the results at the CCSD(T)/BSIII//MP2/BSIII level (6.28 kcal/mol and 4.14 kcal/mol, respectively). B3LYP/BSI provides a poorer geometry for the transition state, especially the H–N–H bond angle (102.7°) compared with that of CCSD/BSII (105.1°). CCSD(T)/BSIII//MP2/BSIII (6.28 kcal/mol) yielded a slightly lower energies than MP2/BSIII (6.45 kcal/mol) because of higher correlation corrections at the CCSD(T) level, which is consistent with the previous work.[71]

3.2 Bond Dissociation of Hydroxylamine

Bond strengths and bond dissociation energies (BDE) are fundamental to chemical reactions, and they can provide deep insight into the stability of chemical compounds. Experimental data on the BDE of **1** are not available, but O–H bond strengths of unhindered dialkylhydroxylamines were determined to be in the range of 72-74 kcal/mol using calorimetric measurements.[73]

Table 4.3. Calculated bond dissociation energies and enthalpies (in kcal/mol) at various levels of theory.

dissociated bond	B3LYP/BSI		MPW1K/BSII		MP2/BSIII		CCSD(T)/BSIII //MP2/BSIII	
	E_0[a]	H_{298}[b]	E_0	H_{298}	E_0	H_{298}	E_0	H_{298}
N–O	60.21	62.03	54.74	56.60	67.22	69.06	59.56	61.40
O–H	67.92	69.31	69.80	71.37	75.44	77.00	74.06	75.61
N–H	82.06	83.42	86.12	87.55	88.46	89.84	86.35	87.73

[a] E_0 = ∑electronic and zero point energies of products - ∑electronic and zero point energies of reactants.
[b] H_{298} = ∑electronic and thermal correction to enthalpy of products - ∑electronic and thermal correction to enthalpy of reactants.

The calculated bond dissociation energies of **1** are shown in Table 4.3. The N–O bond is the weakest bond, and the BDE at 0 K is estimated to be 59.56 kcal/mol at the CCSD(T)/BSIII//MP2/BSIII level, 67.22 kcal/mol at the MP2 level, 54.74 kcal/mol at the MPW1K level, and 60.21 kcal/mol at the B3LYP level. Compared with high-level theoretical calculations (CCSD(T)), density functional theories tend to underestimate BDEs although MPW1K yielded good results on the BDE of N–H, while MP2 tends to overestimate BDEs.

The relatively high energy which is required to break the weakest bond (N–O) suggests that simple bond dissociation reactions of **1** are unlikely to be significant at room temperature. These simple bond breaking reactions cannot explain the highly reactive nature of **1** on its initiation. Therefore, other decomposition reaction pathways must be explored to evaluate its chemical reactivity.

3.3 *Unimolecular Decompositions*

As represented in Scheme 2, eight decomposition pathways of hydroxylamine were proposed including unimolecular and bimolecular reactions. The optimized structures of the species involved in the pathways at the B3LYP level of theory are shown in Figures 4.1-4.3.

Pathway 1 is the isomerization of *cis*-hydroxylamine (**2**) into *trans*-hydroxylamine (**1**), which has been described in the previous section. Pathway 2 involves the isomerization of **1** into ammonia oxide (NH_3O, **3,** see Figure 4.1) via a 1,2-hydrogen shift from the O to N atom. The N–O bond length of NH_3O (1.34 Å) is shorter

than that of *trans*-hydroxylamine (1.45 Å), because NH_3O is a zwitterionic compound ($H_3N^+–O^-$). The electrostatic force between N and O atoms in **3** brings the two atoms closer and shortens the N–O bond length, while in **1**, the repulsion of lone pairs push the N and O atoms away. The total energy of **3** is about 25.45 kcal/mol higher than that of **1** at the CCSD(T)/BSIII//MP2/BSIII level.

The optimized transition state structure (**TS2**) for pathway 2 is also shown in Figure 4.1. This is a central transition state, as evidence by the O–N–H angle of 60º that is about half of the corresponding angle of ammonia oxide (115º). The shifting hydrogen atom is between the N and O atoms with an N–H bond length of 1.09 Å and an O-H bond length of 1.36 Å. A frequency analysis at the B3LYP/BSI level reveals only one imaginary frequency (1442*i* cm^{-1}), which corresponds to the normal mode of hydrogen shifting from the O to N atom. The free energies of the species involved in this pathway are presented in Table 4.4, and the activation energy of this reaction is about 50 kcal/mol at the CCSD(T) and MP2 levels.

Pathway 3 results in hydrogen elimination of NH_3O to form hydrogen gas and a HNO radical. The hydrogen elimination step involves the simultaneous breaking of the N–H and O–H σ bonds, and the formation of a H–H σ bond and an O–N π bond. The optimized geometry of the transition state (**TS3**) for this hydrogen elimination step is represented in Figure 4.1 with two short bonds, H–H (1.27 Å) and N–O (1.23 Å). The rest of the molecule becomes more planar with the formation of the N–O double bond. This is a late transition state based on the N–O bond length (1.23 Å), which is closer to the product nitroxyl (1.20 Å). A frequency calculation on **TS3** had only one imaginary

frequency (1141*i* cm^{-1}) at the B3LYP/BSI level, whose normal mode is consistent with the forming H–H and breaking H–O bonds. Table 4.4 lists the calculated activation barriers of the hydrogen elimination reaction. The activation barrier at MP2/BSIII is 51.36 kcal/mol, and is lower than the MPW1K result (60.08 kcal/mol). CCSD(T) single point energy calculations on the optimized MP2 geometry lowered the barrier by 2.56 kcal/mol. The activation barrier at the CBS-Q level is 52.42 kcal/mol, which is close to the result of CCSD(T)/BSIII//MP2/BSIII.

Pathway 4 involves a hydrogen transfer from the nitrogen to the oxygen atom, forming water and an NH radical that is either in its singlet or triplet state. In this work, both the singlet and triplet pathways are considered. The optimized geometry for singlet NH (**P4**) is shown in Figure 4.1, while the optimized geometry of triplet NH (**P5**) are similar, and their corresponding energies are given in Table 4.4. The NH in triplet state is 47.1 kcal/mol more stable than the singlet state at the CBS-Q level. A singlet transition state (**TS4**) was located with a calculated barrier of 62.22 kcal/mol above **1**. **TS4** is a late transition state, because the N–O bond is very long (1.77 Å) and essentially broken, and H_2O and NH are almost fully formed. A frequency calculation on **TS4** had one imaginary frequency (543*i* cm^{-1}) at the B3LYP/BSI level, whose normal mode is consistent with the hydrogen atom transferring from the N to O atom. The product of the singlet pathway is an imidogen-water complex (**4**), the energy of which is slightly lower than that of **TS4**.

Table 4.4. Relative free energies (ΔG^{o} in kcal/mol at 298 K) for species involved in unimolecular decomposition pathways at various levels of theory.

Structure	B3LYP/BSI	MPW1K/BSII	MP2/BSIII	CCSD(T)/BSIII //MP2/BSIII	CBS-Q
Pathway 2					
1	0.00	0.00	0.00	0.00	0.00
TS2	50.45	51.19	50.01	50.22	48.53
3	28.56	24.95	25.24	25.45	20.43
Pathway 3					
3	28.56	24.95	25.24	25.45	20.43
TS3	67.59	85.03	76.60	74.04	72.84
Barriers	39.03	60.08	51.36	48.59	52.41
P1+P2	24.03	35.29	27.19	25.05	26.07
Pathway 4					
1	0.00	0.00	0.00	0.00	0.00
TS4	62.92	68.00	68.08	64.40	62.22
4	62.94	64.16	64.59	61.47	59.23
P3+P4	85.63	82.16	83.81	70.78	70.52
P3+P5	31.77	24.01	29.86	25.99	23.42

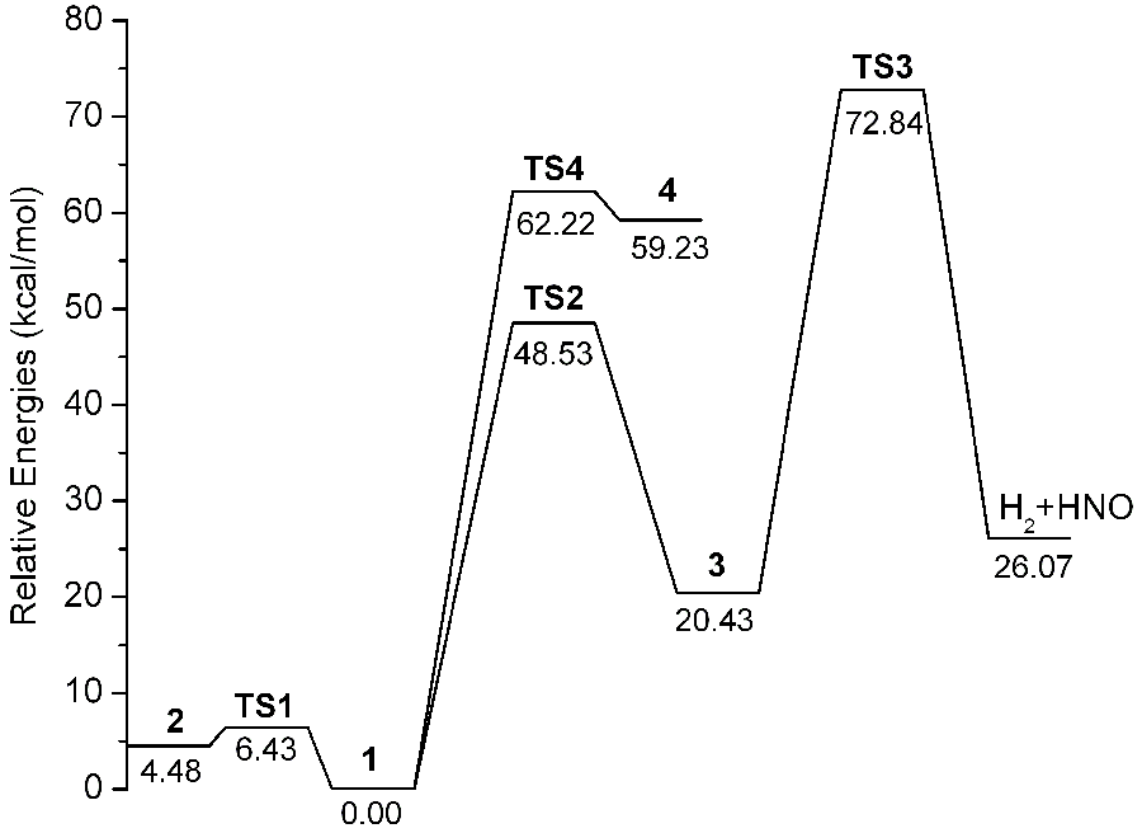

Figure 4.4. Unimolecular decomposition pathways of hydroxylamine. Free energies were calculated at the CBS-Q level.

All of the unimolecular decomposition pathways that were considered so far have high activation barriers, as shown in Figure 4.4. The lowest barrier on the potential energy surfaces is pathway 2, and the calculated barrier for isomerization of hydroxylamine into ammonia oxide is around 50 kcal/mol.

This result is consistent with the experimental and theoretical results proposed by Brönstrup et al.,[74] although they reported some other hydrogen shift pathways with even higher activation energies. Thus, a unimolecular route is also unlikely to be the major decomposition mechanism.

3.4 *Bimolecular Decompositions*

Bimolecular decomposition pathways were explored in search of lower barriers on the potential energy surface. The bimolecular path,[46] as shown in Scheme 1, was proposed to initiate the decomposition, but a transition state could not be located for this reaction, implying that it may not be an elementary reaction. This bimolecular pathway may involve multiple steps: (1) $2NH_2OH \rightarrow NH_2O + NH_3 + OH$; (2) $NH_2O + OH \rightarrow HNO + H_2O$; (3) Radicals NH_2O, NHOH, and OH, react with NH_2OH to propagate the chain reactions and to produce HNO and H_2O.

Pathway 5 involves a hydrogen shift from the O atom of one hydroxylamine molecule to the N atom of another hydroxylamine molecule. Pathway 6 involves a hydrogen shift from one N atom to the N atom of another hydroxylamine molecule. On both decomposition pathways, when the transferring H atom is attacked by the N atom of another hydroxylamine and forms ammonia, the N–O bond of the attacking

hydroxylamine molecule is broken (see **TS5** and **TS6** in Figure 4.2). The molecular structures of the species involved in the pathways 5 and 6, which were optimized at the B3LYP level of theory are shown in Figure 4.2, and the free energies of the species are presented in Table 4.5. The frequency calculations on **TS5** had **TS6** result only one imaginary frequency at the B3LYP/BSI level, 472*i* cm^{-1}, and 563*i* cm^{-1}, respectively. Because the transition states in pathways 5 and 6 are open shell singlet systems, unrestricted density functional and coupled-cluster UCCSD(T) methods were used to optimize the structures and to calculate the free energies, respectively. The geometry optimizations were carried out using either the UB3LYP/BSI or UMPW1K/BSII levels of theory.

Although the energies differ significantly at the B3LYP/BSI and MPW1K/BSII levels (60.50 kcal/mol and 76.72 kcal/mol, respectively, in pathway 5, and 64.54 kcal/mol and 89.26 kcal/mol, respectively, in pathway 6), the UCCSD(T) single point energy calculations provided very close results (50.59 kcal/mol and 45.89 kcal/mol, respectively, in pathway 5, and 40.10 kcal/mol and 47.20 kcal/mol, respectively, in pathway 6) based on the optimized structures and thermal corrections at the corresponding density functional theories. The activation barriers at the UCCSD(T) level are significantly lower than those using density functional theories, especially compared to the MPW1K level of theory. Solvent effects on pathways 5 and 6 will be addressed later.

In decomposition pathways 7 and 8, two hydrogen atoms shift between two hydroxylamine molecules, forming ammonia oxide. Two transition states, **TS7** and **TS8**, optimized at the B3LYP level of theory (with only one imaginary frequency, 1166*i* cm^{-1} for **TS7**, and 1430*i* cm^{-1} for **TS8**), are shown in Figure 4.3.

Analogous to the transition state in pathway 5 (**TS5**), the H atom in the OH group transfers to the N atom of another hydroxylamine molecule; meanwhile, the electron repulsion weakens the O–H bond in **TS7**, forming ammonia oxide, instead of breaking the O–N bond in **TS5**. The H atom in the weakened O–H bond transfers to another O atom, forming a new hydroxylamine molecule. The difference between pathways 7 and 8 is the conformation of the formed hydroxylamine molecule, and the H contributing groups in pathway 8 are NH_2 and OH, instead of two OH groups in pathway 7.

Table 4.5. Relative free energies (ΔG^{o} in kcal/mol at 298 K) for species involved in bimolecular decomposition pathways at various levels of theory.

Structure	B3LYP/BSI	MPW1K/BSII	CCSD(T)/BSII //B3LYP/BSI	CCSD(T)/BSII //MPW1K/BSII
Pathway 5				
1+1 (**5**)	0.00 (0.00)[a]	0.00 (0.00)	(0.00)	(0.00)
TS5	60.63 (60.50)	84.23 (76.72)	(50.59)	(45.83)
P6+P7+P8 (**6**)	19.14 (17.13)	14.09 (13.14)	(24.42)	(19.25)
Pathway 6				
1+1 (**7**)	0.00 (0.00)	0.00 (0.00)	(0.00)	(0.00)
TS6	64.67 (64.54)	92.28 (89.26)	(40.10)	(47.20)
P7+P8+P9 (**8**)	27.84 (22.93)	30.49 (26.02)	(31.15)	(28.11)
Pathway 7				
1+1 (**9**)	0.00 (0.00)	0.00 (0.00)	(0.00)	(0.00)
TS7	22.44 (22.34)	27.93 (24.92)	(26.17)	(26.94)
1+3 (**10**)	28.58 (16.10)	24.59 (14.89)	(15.47)	(16.36)
Pathway 8				
1+1 (**11**)	0.00 (0.00)	0.00 (0.00)	(0.00)	(0.00)
TS8	31.16 (29.74)	34.76 (31.73)	(35.74)	(36.05)
2+3 (**12**)	33.06 (24.69)	30.28 (23.20)	(25.04)	(23.20)

[a] Species in parenthesis are reactant wells, transition state wells or product wells including the hydrogen bond effect.

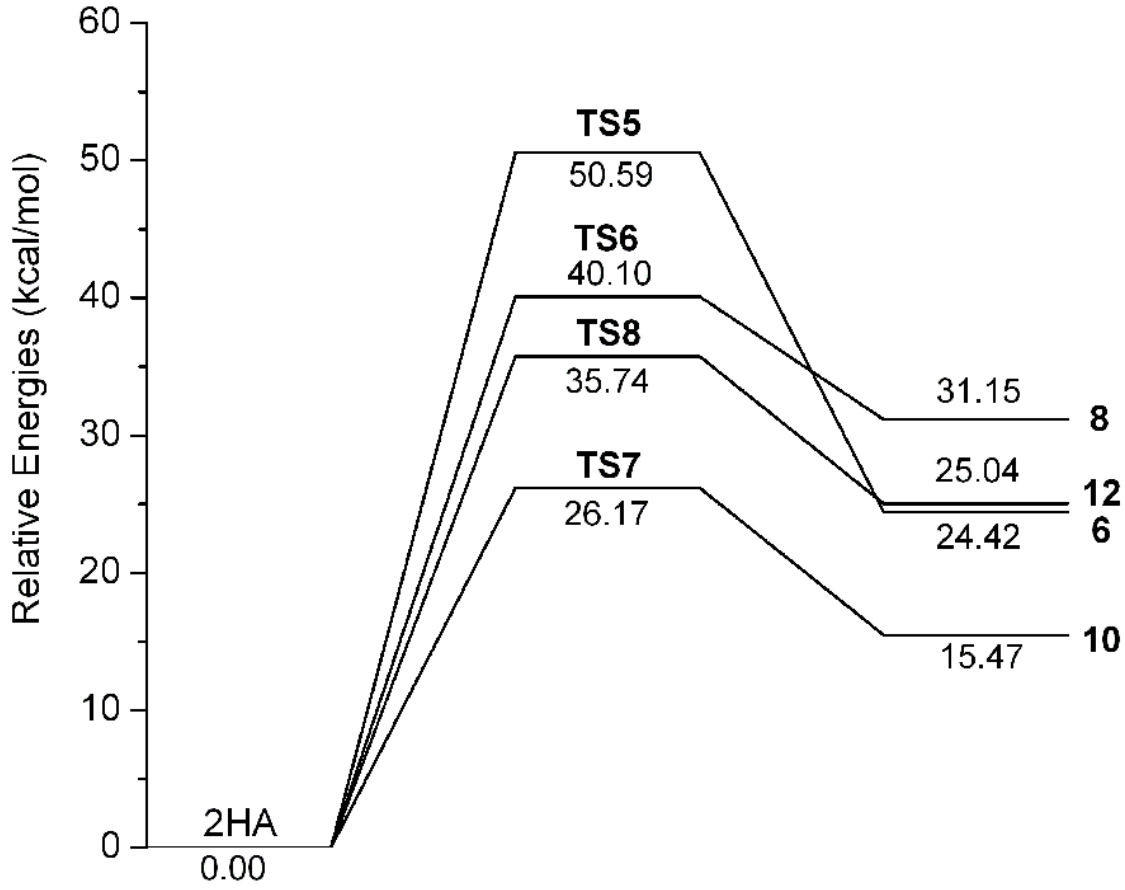

Figure 4.5. Bimolecular decomposition pathways of hydroxylamine. Free energies were calculated at the CCSD(T)/BSII//B3LYP/BSI level.

As shown in Table 4.5, the activation barrier of pathway 7 is about 22 kcal/mol at the B3LYP level, which is significantly lower than that of the unimolecular reaction pathway 2 (50 kcal/mol). It should be noted that the barrier for the reverse reaction ($NH_3O \rightarrow NH_2OH$) is very low in the gas-phase, which may contribute to the difficulty of detecting ammonia oxide by experimental methods, because ammonia oxide might easily isomerize into hydroxylamine.

3.5 Solvent Effect

It is important to consider solvent effects on the hydroxylamine decomposition pathways, because hydroxylamine is manufactured and used in aqueous solutions. The gas phase reaction pathway analysis shows that pathway 7 is the most likely to occur due to its lowest activation barrier of 26 kcal/mol, as shown in Figure 4.5.

This bimolecular reaction involves two hydrogen shifts and produces ammonia oxide, which is less stable than hydroxylamine. Pathways 5 and 6 may also be important, because they produce radicals OH, NHOH, and NH_2O. These radicals can react with hydroxylamine to propagate the chain reactions. Therefore, solvent effects were considered for pathways 5-7 to determine if these decomposition pathways are more favorable in the solution.

Table 4.6. Solvent effects on free energies (in kcal/mol at 298 K) for species involved in pathway 7 at the MPW1K/BSII level of theory.

Structure	No solvent	NH_2OH	H_2O	$2H_2O$	$3H_2O$	PCM
9	0.00	0.00	0.00	0.00	0.00	0.00
TS7	24.92	23.85	18.94	20.10	16.10	16.81
10	14.89	13.93	10.89	8.47	4.23	4.32

The clusters of hydroxylamine and water were used to simulate the solvation effects. All the structures in pathway 7 were fully optimized at the MPW1K/BSII level, and the energies are shown in Table 4.6. The inclusion of solvent molecules reduces the activation barriers, and water (18.94 kcal/mol) can stabilize the transition state better than hydroxylamine (23.85 kcal/mol). With two water molecules (20.10 kcal/mol) included, the activation barrier becomes higher than the ones with one (18.94 kcal/mol) or three water molecules (16.10 kcal/mol), because the reactant consisting of two water and two hydroxylamine molecules poses a symmetric structure and is stabilized significantly. The free energy of reaction decreases with an increasing number of water molecules. With three water molecules as solvent, the free energy of reaction becomes 4.23 kcal/mol.

The results show that the solvent effect of water is evident in the small clusters containing only a few water molecules. Continuum models describing solute-solvent interactions were also used to study the decomposition pathway. Single point energy calculations were conducted using the PCM method with Klamt's radii and an iterative solution[75, 76] at the MPW1K/BSII level, based on the optimized structure at the same level of theory. The free energy of activation at 298 K including the thermal correction for **TS7** is 16.81 kcal/mol using the CPCM method, which is very close to the result of 16.10 kcal/mol using a cluster containing three water molecules. However, the solvent effect of a small water cluster converges more quickly than that of bulk water.

The solvent effects on pathways 5 and 6 were also studied to see if these pathways become favorable in aqueous solution. For pathway 5, the free energy of

activation and the free energy of reaction at 298 K (including thermal corrections) are 100.17 and 1.09 kcal/mol, respectively, at the CCSD(T)/BSII//B3LYP/BSI level using the CPCM model. The CPCM model was also used to simulate solvent effects at the CCSD(T)/BSII//B3LYP/BSI level for pathway 6, and the free energy of activation and the free energy of reaction at 298 K (including thermal corrections) are 39.75 and 11.27 kcal/mol, respectively. Because of significantly higher activation energies than that of pathway 7 (16 kcal/mol), pathways 5 and 6 are unlikely to occur at room temperature.

4. Conclusions

Hydroxylamine decomposition pathways were investigated using density functional and *ab initio* methods. In this work, both unimolecular and bimolecular reactions were analyzed to locate the pathway with a low activation barrier. Simple bond dissociations and unimolecular hydrogen shift or elimination reactions require high activation energies.

Several bimolecular pathways, however, were found to have lower activation barriers than unimolecular reactions: 1) in pathways 5 and 6, a hydrogen shift between two hydroxylamine molecules can induce the dissociation of the N–O bond and produce two radicals, and 2) in pathways 7 and 8, two hydrogen shifts can facilitate the isomerization of hydroxylamine to ammonia oxide. Accurate calculations show that the lowest gas-phase activation barrier for the bimolecular isomerization step is about 26 kcal/mol.

Although accurate gas-phase decomposition pathway analysis can provide a good reference, solvent effects on the potential energy surface were investigated using cluster and continuum methods. Water solvent can stabilize the transition states and lower the activation barriers and the free energies of reactions. In aqueous solutions, the bimolecular isomerization step is the most favorable pathway with an energy barrier of only 16 kcal/mol. The theoretical study shows the potential formation of ammonia oxide in solutions. The N–O bond dissociation enthalpy of NH_3O ($NH_3O \rightarrow NH_3 + {}^3O$) at 298 K was calculated to be 35 kcal/mol at the G2 level of theory.[77] Research on the detection of NH_3O, and possible decomposition reactions induced by NH_3O will be conducted in the future.

CHAPTER V

REACTIVITY OF ENERGETIC MATERIALS *

1. Background

In recent years, investigations on synthesis and application of energetic materials have been generating extensive interest among researchers.[78] These materials, which contain multiple NO_2 functional groups, are capable of rapid chemical decomposition with large energy release and therefore are often used as fuels, high explosives, and propellants.[79] These materials are representative of layered wide band gap molecular crystals and have favorable properties such as good heat resistivity, high heat of formation, low sensitivity, and thus, studying their electronic structures and electronic excitations is of fundamental interest.

The macroscopic properties of energetic materials have been studied for years and considered to be well understood.[80] However, the micro-scale mechanisms and conditions that favor initiation of chemistry in these materials are yet to be established. The mechanism study of thermal decomposition has attracted the interest of both chemical engineers and materials scientists because it is essential to engineering design and fundamental to the design and optimization of materials.[81,82]

In general, the initial steps in the thermal decompositions of energetic materials are considered very important in the reaction mechanism, which can be caused by a thermal heat, shock, or mechanical impact. Once the initial steps are triggered, the material undergoes a rapid chemical reaction. The initial reactions have been studied for several typical energetic materials, such as RDX (hexahydro-1,3,5,-trinitro-*s*-triazine),[83] FOX-7 (1,1-diamino-2,2-dinitroethylene),[84] and TNAZ (1,3,3,-trinitroazetidine),[85] which typically involve the fission or transformation of the weakest C–N bonds. However, the overall decomposition mechanisms for energetic materials are still not well understood, which is critical in determining the fundamental kinetics of high explosives.

The complexity and compositional variability of energetic materials can be an obstacle to the study of fundamental reaction mechanism and kinetic modeling. For this reason, the development of simple nitro compounds that closely match the behavior of general energetic materials is critical. A systematic study of simple nitro compounds may facilitate the determination of basic bond dissociation energies of the various types of C–N bonds and may reveal the general mechanistic features for the corresponding energetic materials.

Following this line of thought, nitroethane ($C_2H_5NO_2$) has been chosen as a representative nitro compound in this work. Nitroethane have been extensively investigated over the past few years.[86] For example, Spokes and Benson performed a very low-pressure pyrolysis study of the decomposition of nitroethane, and they concluded that the major products of these reactions were olefins and HNO_2 through a concerted molecular elimination (CME) mechanism.[87] The remaining products were

assigned to the decomposition of HNO_2 and the activation energy was determined as 45 kcal/mol by Benson et al.[88]

However, later other researchers pointed out that the decomposition via C–N bond fission is more favorable than the CME mechanism.[89] In 1986, an infrared multi-photon dissociation study of the decomposition of nitromethane was conducted by Wodtke et al.[90] The activation barrier for nitroethane was estimated as 46 kcal/mol, in agreement with the CME mechanism. However, several assumptions were made to obtain those results, due to the lack of thermodynamic and kinetic data.

Recently, Denis et al. conducted a density functional study of the decomposition pathways of nitroethane at the B3LYP level.[91] It was found that the CME pathway is the most favorable decomposition channel, in addition to other important mechanistic routes. The activation energy was calculated to be 42.0 kcal/mol, which is consistent with the activation energies predicted by Benson et al. on the basis of experimental information.

To the best our knowledge, little work has been conducted on the detailed mechanism and kinetics of the decomposition of nitroethane. In this chapter, we report the results of a theoretical and experimental study of the kinetics of thermal decomposition for nitroethane. The thermal decomposition was studied experimentally using automatic pressure tracking adiabatic calorimeter (APTAC), followed by the determination of final products using gas chromatography (GC). The motivation of this work is to establish a reaction mechanism specifically for nitroethane, which can be extended to better understand the modeling and engineering of other energetic materials.

2. Experimental Section

Chemicals. Nitroethane was obtained from Aldrich and used as received. It has a stated purity of 98%, which is consistent with our GC–MS analysis of unheated samples of the nitroethane.

Apparatus. The thermal decomposition behavior of nitroethane was measured using the automatic pressure tracking adiabatic calorimeter (APTAC) in the temperature range of 250–500 °C. The APTAC can be operated with temperatures up to 500 °C and pressures ranging from vacuum to 2000 psia, and can detect exotherms with heat generation rates from 0.04 to 400 °C/min. In this work, the Heat-Wait-Search (HWS) operation mode was used. The reactant in the reaction vessel was firstly heated to the start temperature, 250 °C, with heating rate of 2 °C/min. Then the system was stabilized for about 10 min, followed by a search for exotherms. If not, the reactant was heated to the next target temperature, 260 °C, which is 10 °C higher than previous temperature. If the self-heating rate of the sample was greater than a preset threshold (0.05 °C/min), the apparatus tracked the reaction adiabatically until the reaction ended or one of the shutdown criteria was met. Details of APTAC equipment and its HWS mode are also available in the previous publication.

The distributions of final products under different temperatures were measured using HP 6890N gas chromatography (GC) equipped with a flame ionization detector (FID). The experimental setup is shown in Figure 5.1. Helium was used as the carrier gas. The flow rate of the nitroethane was controlled by a feed pump and set as 5 mL/hour. Note that two syringes were used, so the actual flow rate was 10 mL/hour. The

nitrogen flow rate was controlled by a mass flow meter. The micro-reactor which consisted a stainless steel tubing was connected directly to GC through the transfer line and GC split injection inlet. A temperature program was performed at an initial isothermal separation at 50 ˚C for 8 min, followed by a 10 ˚C/min gradient to 220 ˚C. This final temperature was held constant for 1 min.

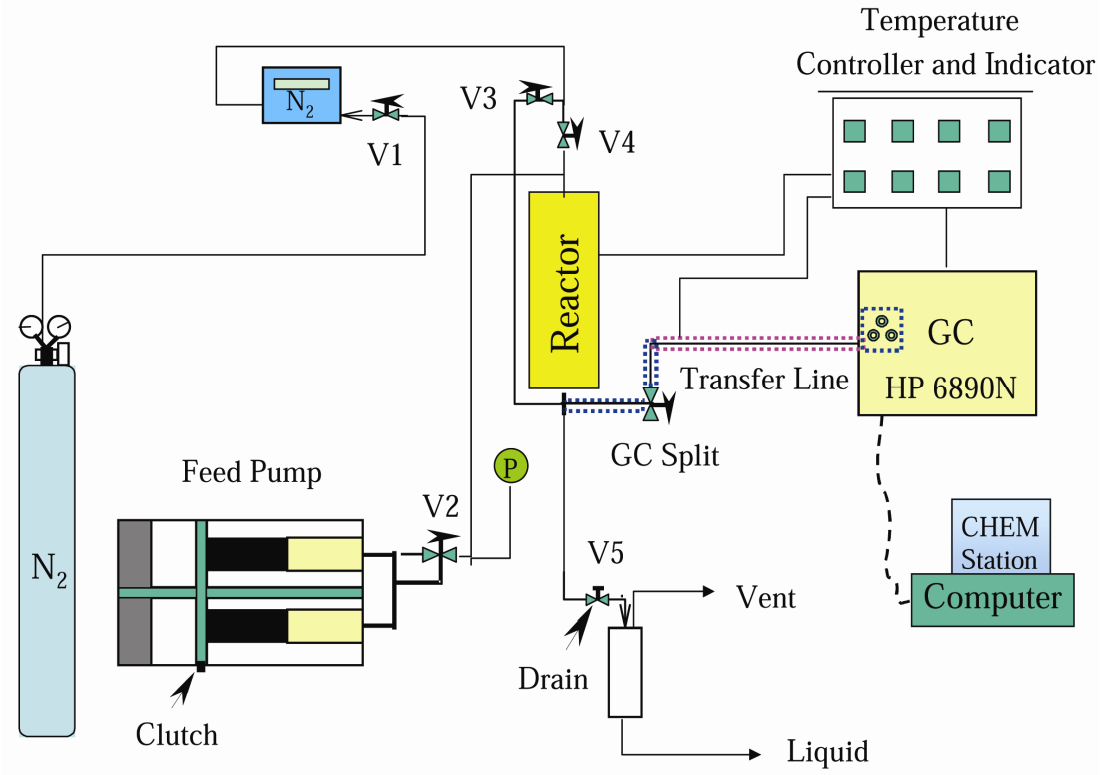

Figure 5.1. Experiment setup of GC analysis for the decomposition of nitroethane.

3. Computational Details

All calculations on the initial decomposition steps were performed using the Gaussian 03 programs. A B3LYP method was used for gas-phase geometry optimizations and frequency calculations with Pople-style basis sets. Calculating the vibrational frequencies at the B3LYP/6-31+G(d) level of theory and noting the number of imaginary frequency of 1 confirmed the nature of all transition state structures. The calculation of intrinsic reaction path was also conducted to follow the reaction pathways and used to check whether a transition state connects two minima of interest on the potential energy surface. Relative energies were reported in kcal/mol. Representations of the transition states, shown in Figures 5.2, were created using the JIMP 2 program.[92]

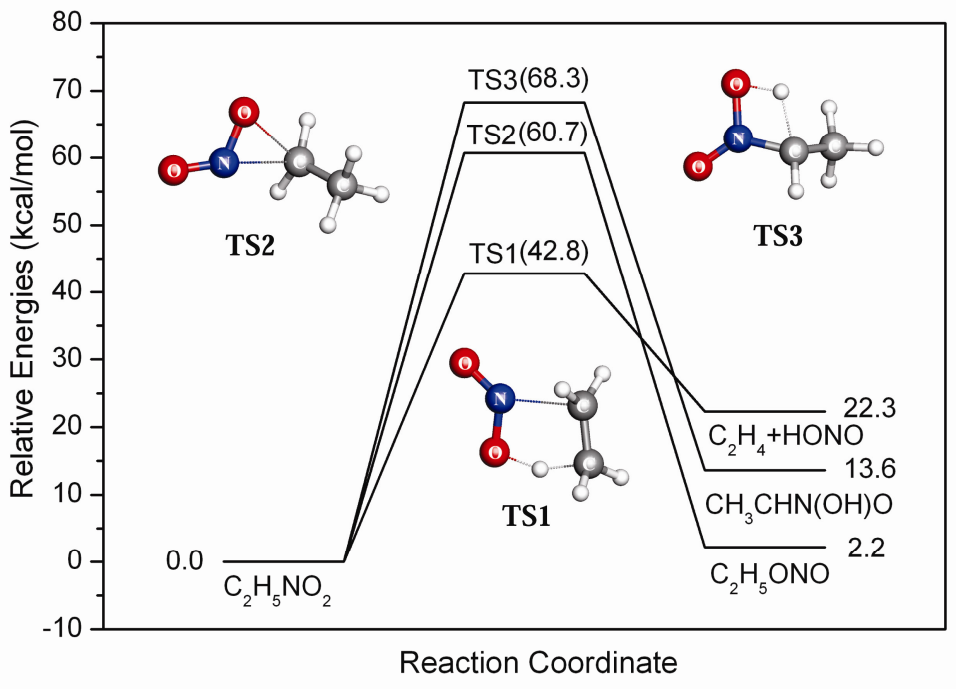

Figure 5.2. Initial decomposition pathways on the potential energy surface of NE.

4. Results and Discussion

4.1 Determination of the Arrhenius Parameters

Adiabatic calorimetry is an extremely useful tool to assess thermal decomposition of nitro compounds. It can minimize heat losses by keeping the temperature of the surroundings close to that of the sample. In the present study, the calorimetric measurements were conducted in a glass sample cell of 100 ml volume in the APTAC. The HWS mode was employed to determine the overall decomposition behavior of nitroethane. The experimental results are shown in Figure 5.3.

Decomposition of nitroethane starts at 270 °C and the temperature increases slowly until approximately 280 °C, at which point the temperature suddenly increases very rapidly to a maximum temperature of 388 °C. The temperature profile of nitroethane appears to consist of two stages: a slow initiation stage followed by a fast explosion stage.

The decomposition of nitroethane has been described as a first order reaction.[93] Therefore, the reaction rate can be expressed as

$$-r_A = kC_A \tag{5.1}$$

where r_A is the reaction rate (mol/m^3·s), k is the rate constant (1/s for the first order reaction), and C_A is the concentration (mol/m^3). In this study, the following assumptions were made to obtain the overall reaction model and the Arrhenius parameters: (1) the reaction system is assumed to be adiabatic, and therefore heat losses are negligible; (2) the mass and volume of the liquid phase remain constant (i.e. evaporation losses are

neglected). The specific heat of the liquid is considered to be constant during the reaction; (3) a uniform temperature exists throughout the liquid phase.

Based on these assumptions, the heat balance equation can be written as follows

$$(-\Delta H_r)(-r_A)V + \Phi m C_p \frac{dT}{dt} = 0 \tag{5.2}$$

where ΔH_r is the heat of reaction (kcal/mol), V is the reaction volume (m^3), m and C_p are mass (kg) and specific heat capacity (cal/kg·K) of the chemical compound, respectively. T is the absolute temperature (K) and t is the time (s). Φ is the thermal inertia coefficient, which is larger than but close to 1 for typical industrial reactors. In this work, to simplify the kinetic model, $\Phi = 1$ will be chosen, which is the worse case for a thermal runaway reaction. Additionally, the heat of reaction can be expressed as

$$\Delta H_r = \int_T^{T_m} C_p dT = C_p (T_m - T) \tag{5.3}$$

where T_m is the maximum temperature, which is 388 °C in this work. Combining Equations (1), (2) and (3) gives

$$\frac{dT}{dt} = k(T_m - T) \tag{5.4}$$

The rate constant k can be described by the Arrhenius equation

$$k = A \exp(-\frac{E_a}{RT}) \tag{5.5}$$

where A is the frequency factor, E_a is the activation energy (kcal/mol), and R is the gas constant (cal/mol·K). Therefore, the overall reaction model can be represented as

$$\frac{dT}{dt} = A \exp(-\frac{E_a}{RT})(T_m - T) \tag{5.6}$$

Using the Matlab® ODE solver or Polymath® program, the experimental data were fitted to the overall kinetic model (Equation 5.6) to give the frequency factor and apparent activation energy as $10^{13.5\pm0.2}$ and 46.2±0.5 kcal/mol, respectively (see Figure 5.3). The rate constant can be expressed as

$$k = 10^{13.5\pm0.2} \exp\left(\frac{-46.2 \pm 0.5 \text{ kcal/mol}}{RT}\right) \tag{5.7}$$

Previous studies using other analytical tools have shown that the decomposition of nitroethane is a first order reaction with overall activation energy of 47 kcal/mol, which is in agreement with our results.

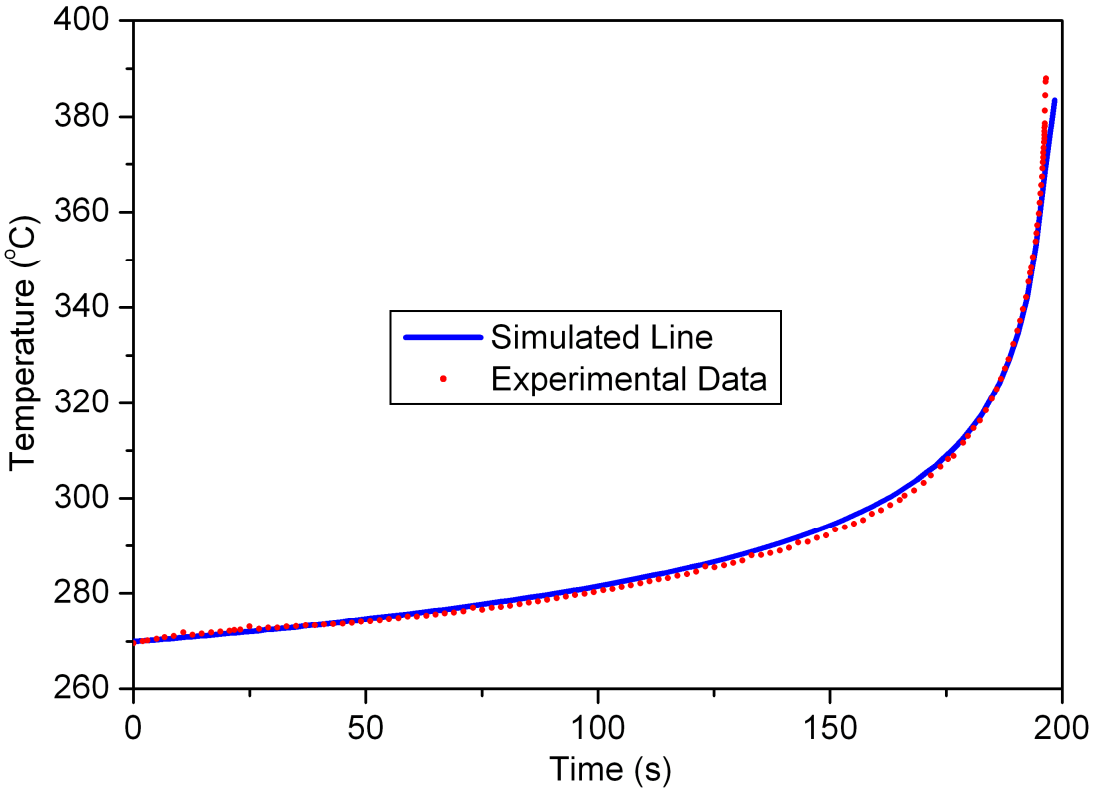

Figure 5.3. APTAC experimental results of thermal decomposition of nitroethane and the overall kinetic model simulation.

4.2 Initial Steps

The studies of initial steps are always critical to develop the decomposition mechanism of energetic materials.[94] In order to elucidate further the decomposition mechanisms, firstly, we simulate relevant initial steps, such as HONO elimination and nitro-nitrite isomerization as well as rupture of C–NO_2, which are shown in Equation 5.8. It should be noted that the results of this work apply solely to the gas phase decomposition of nitroethane and therefore they cannot be simply extrapolated to solid state decomposition process.

$$\begin{aligned} CH_3CH_2NO_2 &\longrightarrow CH_2CH_2 + HONO \\ CH_3CH_2NO_2 &\longrightarrow CH_3CH_2ONO \\ CH_3CH_2NO_2 &\longrightarrow CH_3CH(OH)NO \\ CH_3CH_2NO_2 &\longrightarrow CH_3CH_2 + NO_2 \end{aligned} \qquad (5.8)$$

The first pathway, which is called CME mechanism, is known to take place at moderate temperatures. This mechanism proceeds through a five-member cyclic transition state to give the corresponding olefin and HONO. The transition state (**TS1**, Figure 5.2) was optimized at the B3LYP/6-31+G(d) level of theory. Atoms involved in the **TS1** are nitrogen, oxygen of the NO_2 group, the C atom bearing the nitro group, the adjacent carbon, and the hydrogen that is transferred to yield HONO. According to the geometrical parameters, the **TS1** is a five-member planar ring. The activation energy was calculated to be 42.8 kcal/mol at the same level of theory, which is in good agreement with the experimental value.

The second step involves the isomerization of C–NO_2 to a C–ONO fragment. The isomerization reaction occurs through a pseudo-rotation of the NO_2 group. From the three-center transition state structure (**TS2,** Figure 5.2), the CH_2 group is almost planar and the NO_2 group is so arranged that the N and one of the O atoms are almost at the same distance from the C in the CH_2 group. The activation barrier for this isomerization is 60.7 kcal/mol at the B3LYP/6-31+G(d) level, about 18 kcal/mol higher than the **TS1** for the CME mechanism. After the CONO isomer is formed, the CO–NO bond can be cleaved with formation of the NO species. The third step is another isomerization of nitroethane to $CH_3CHN(OH)O$. The activation energy of the transition state structure **TS3** is very high, 68.3 kcal/mol, making this isomerization unlikely to occur. In order to simplify the decomposition mechanism, the third initial step was not considered here.

The last pathway is the rupture of C–NO_2 bond, which is often suggested as an initial step in the thermal decomposition of nitro compounds, because the attachment of nitro groups is relatively weak.[95] The C–N bond dissociates without an apparent transition state structure, and affords two radicals. The calculated reaction enthalpy for gas-phase nitroethane to form radicals is 56.1 kcal/mol at the B3LYP/6-31+G(d) level.

To better understand the C–NO_2 bond rupture, a detailed reaction profile was calculated as a function of C–NO_2 bond length. For each fixed C–NO_2 distance, the system was allowed to relax to a minimum energy configuration. Calculations were performed for both singlet and triplet electronic configurations at the B3LYP/6-31+G(d) level. The results are shown in Figure 5.4, and clearly show that singlet calculations are not adequate for predicting radical formation. As the bond is stretched, the predicted

energy is increasing even though the C–N bond length reaches 4.5 Å. Triplet calculations appear to be more successful at modeling radical formation via C–NO_2 bond rupture. From an optimum configuration, when the C–N bond length is 1.52 Å, the triplet energy increases by nearly 23 kcal/mol, to a maximum point at the C–N bond length of 2.0 Å. Beyond 2.8 Å, the triplet energy settles to a value of 60 kcal/mol, which is close to the calculated reaction enthalpy for radical formation (56.1 kcal/mol). These calculations indicate that radical formation in nitroethane is a two-step process: (1) singlet to triplet excitation; (2) further excitation to a transition state. These results are similar to the DFT calculations of nitromethane by Manaa et al.[96,97]

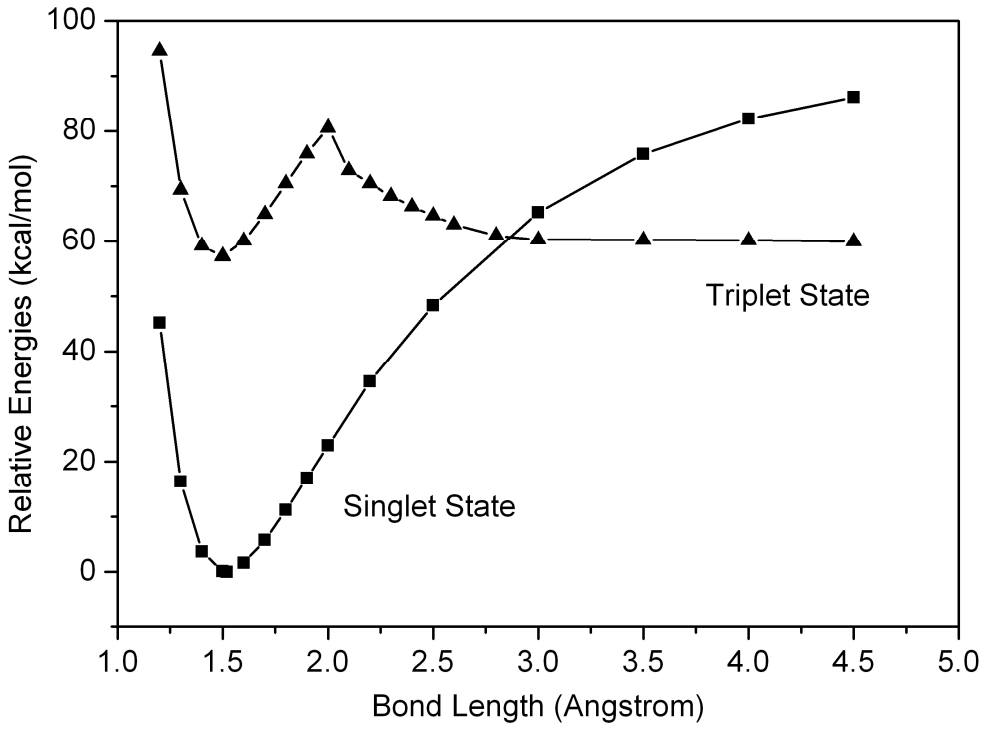

Figure 5.4. Reaction pathways for C–NO_2 bond scission in nitroethane. All energies are given relative to the minimum energy of the singlet ground state.

4.3 Decomposition Mechanism

A complete decomposition mechanism for the conversion of nitroethane was presented in Figure 5.5. To fully describe the decomposition pathways over wide temperature ranges, many elementary reaction steps were included in the mechanism. Note that there are a number of active free radicals that play very important roles at various stages of the conversion.

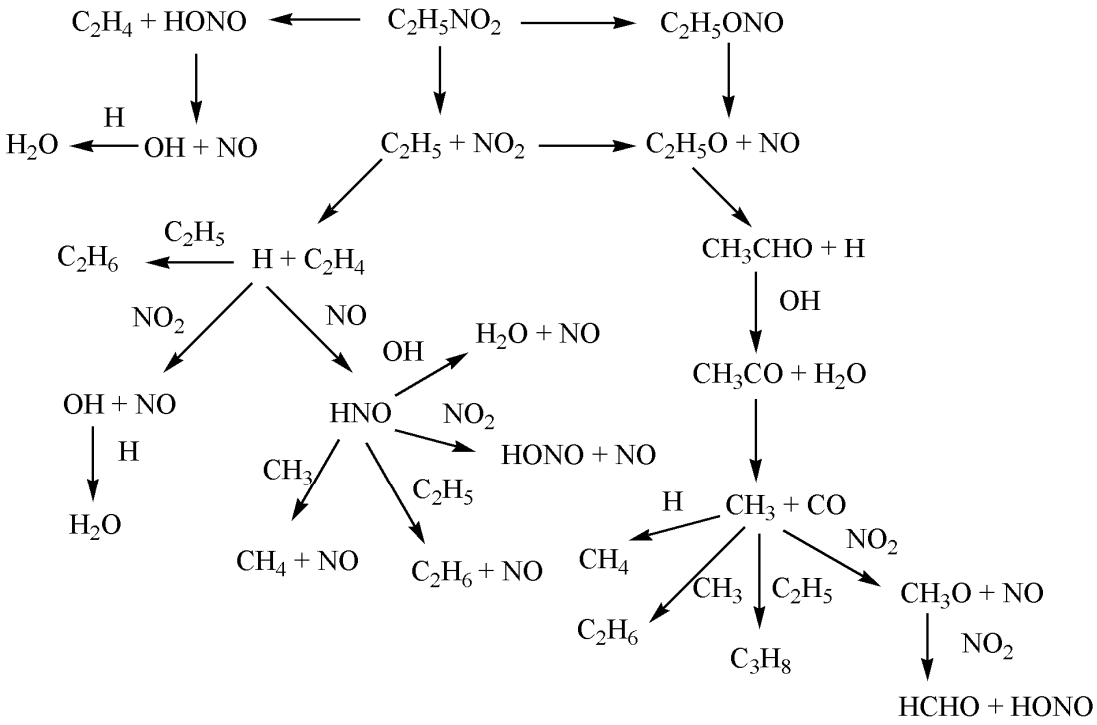

Figure 5.5. Reaction sequence in the thermal decomposition of nitroethane.

At the initial stage, only three pathways were considered, as described in the last section. Recombinations and reactions between radicals and the parent compound lead to the formation of other transient species and stable final products. The rate constants (shown in Table 5.1) for these reactions are available in the NIST Chemical Kinetics Database.[98] The proposed mechanism in Table 5.1 were applied and kinetic behaviors of all chemical species were numerically solved with the Matlab® ODE solver or Polymath® program. The following final gaseous products were predicted: NO, C_2H_4, H_2O, HCHO, CO, CH_4 and C_2H_6.

The distributions of $C_2H_5NO_2$, NO, and C_2H_4 derived by numerical simulations at 800 K are presented in Figure 5.6. The simulated decay curve of nitroethane remains the first order, but deviates somewhat from the experimental curve from the first order rate constant in equation (5.7). As reported previously, C_2H_4 and NO are the most abundant species in the product mixtures. Both C_2H_4 and NO are increasing with the reaction time and reach steady state.

However, in steady state, the C_2H_4 concentration is larger than that of NO for the low-temperature decompositions (< 720±20 K) as shown in Figure 5.7. For high-temperature decompositions, the NO concentration is larger, which indicates that C–NO_2 bond fission remains dominant when temperature is higher than 720±20 K.

Table 5.1. Thermal decomposition mechanism of nitroethane.

No.	Reaction	A	n	E_a	Order
1	$C_2H_5NO_2 \rightarrow C_2H_4 + HONO$	5.60×10^{11}	0	180	1
2	$C_2H_5NO_2 \rightarrow C_2H_5 + NO_2$	1.00×10^{13}	0	197	1
3	$C_2H_5NO_2 \rightarrow C_2H_5ONO$	6.25×10^{12}	1	254	1
4	$HONO \rightarrow OH + NO$	1.09×10^{16}	-1.23	208	1
5	$C_2H_5 \rightarrow H + C_2H_4$	1.58×10^{13}	0	159	1
6	$H + NO \rightarrow HNO$	1.47×10^{14}	-0.41	0	2
7	$HNO + OH \rightarrow H_2O + NO$	4.82×10^{13}	0	4.16	2
8	$HNO + NO_2 \rightarrow HONO + NO$	6.02×10^{11}	0	8.31	2
9	$HNO + CH_3 \rightarrow CH_4 + NO$	2.00×10^{12}	0	0	2
10	$HNO + C_2H_5 \rightarrow C_2H_6 + NO$	1.00×10^{12}	0	0	2
11	$H + NO_2 \rightarrow OH + NO$	1.32×10^{14}	0	1.51	2
12	$H + C_2H_5 \rightarrow C_2H_6$	1.00×10^{14}	0	0	2
13	$H + CH_3 \rightarrow CH_4$	5.20×10^{14}	-0.60	1.57	2
14	$H + OH \rightarrow H_2O$	2.09×10^{17}	0	0	3
15	$C_2H_5ONO \rightarrow C_2H_5O + NO$	1.00×10^{16}	0	175	1
16	$C_2H_5O \rightarrow CH_3CHO + H$	1.51×10^{10}	0	98.11	1
17	$C_2H_5 + NO_2 \rightarrow C_2H_5ONO$	5.68×10^{12}	0	0	2
18	$CH_3CHO + OH \rightarrow CH_3CO + H_2O$	1.00×10^{13}	0	0	2
19	$CH_3CO \rightarrow CH_3 + CO$	4.04×10^{15}	0	57.54	2
20	$CH_3 + CH_3 \rightarrow C_2H_6$	1.41×10^{14}	0	5.9	2
21	$CH_3 + C_2H_5 \rightarrow C_3H_8$	2.51×10^{13}	0	1.67	2
22	$CH_3 + NO_2 \rightarrow CH_3O + NO$	2.50×10^{12}	0	0	2
23	$CH_3O + NO_2 \rightarrow HCHO + HONO$	1.00×10^{11}	0	0	2

[a] Rate constants are in the form $k(T) = A(T/298)^n\exp(-E_a/RT)$ with the unit of s^{-1} for first order reactions, $m^3mol^{-1}s^{-1}$ for second order reactions, and $m^6mol^{-2}s^{-1}$ for third order reactions. E_a is in kJ/mol.

[b] All the data are available from NIST Chemical Kinetics Database.

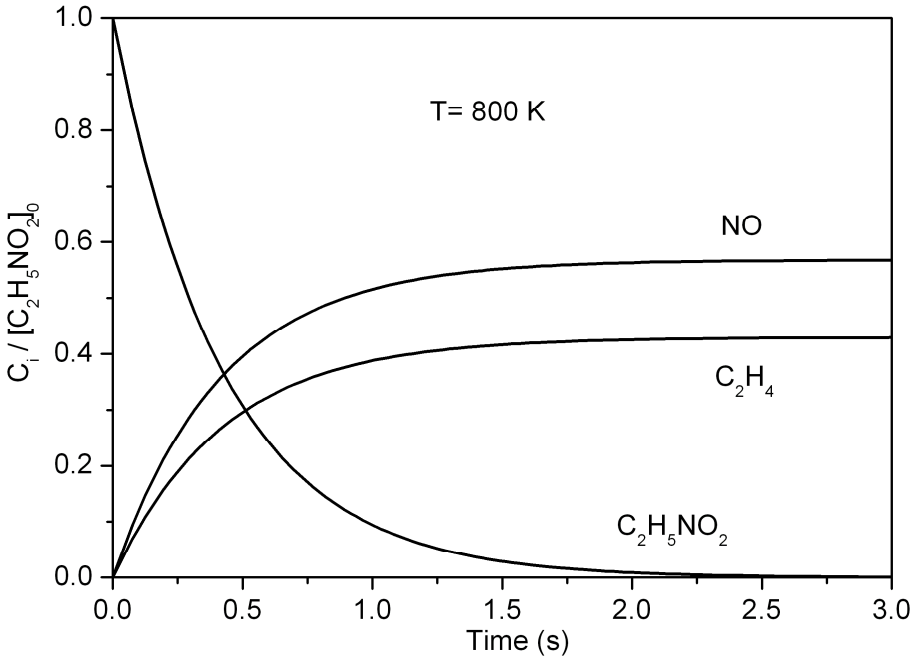

Figure 5.6. The computed relative concentration of major products vs time at 800 K, per the mechanism in Table 5.1.

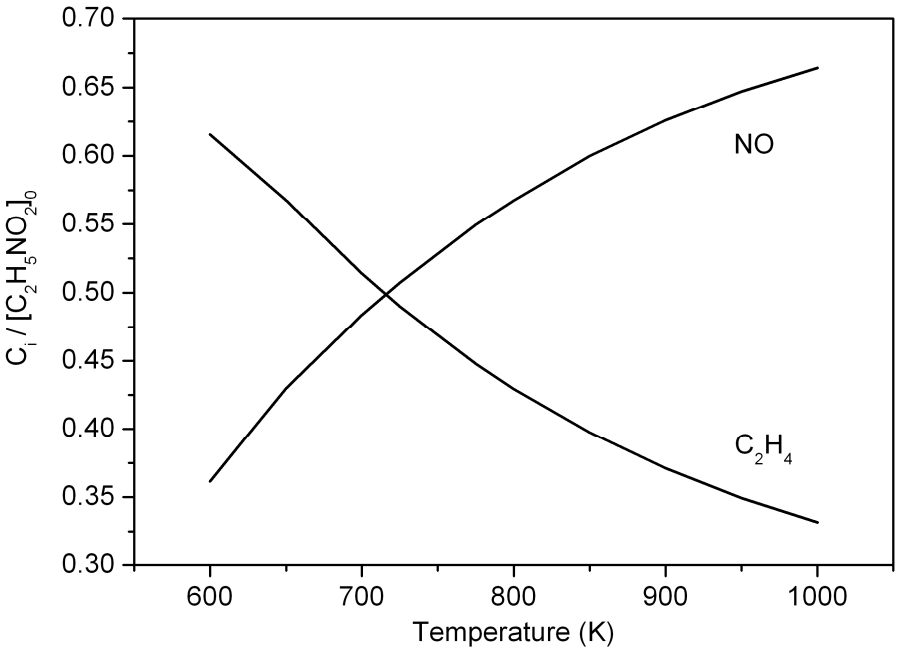

Figure 5.7. The relative simulated concentration of C_2H_4 and NO at different temperatures.

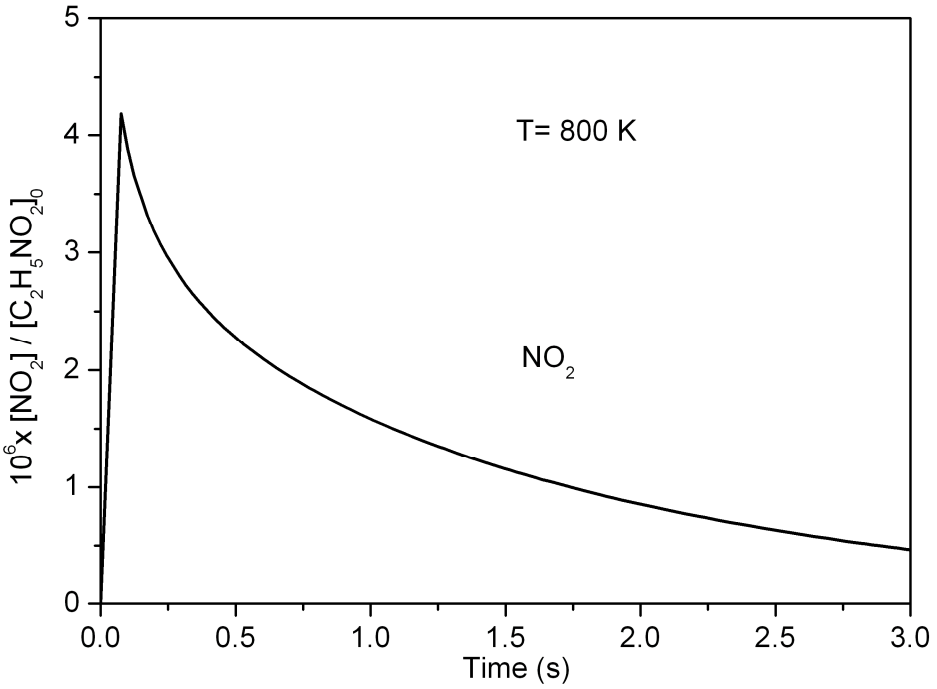

Figure 5.8. Computed concentration of NO_2 vs time at 800 K, per the mechanism.

It should be noted that both radicals NO_2 and C_2H_5 are the most important intermediates in the decomposition mechanism of nitroethane. A clear understanding of their kinetics is crucial for elucidating the mechanism of the overall conversion. The NO_2 concentration vs. time using computer simulations during the decomposition at 800 K was shown in Figure 5.8. The NO_2 profiles resemble those observed in the decomposition of nitromethane, suggesting similarities in the mechanisms of the two systems. NO_2 was produced very fast and consumed relatively slowly and the final NO_2 concentration was very low. This is consistent with the GC spectra of the product mixtures, which show no NO_2 peak. The C_2H_5 profiles are similar to NO_2, which was also produced very fast and the final concentration was approach 0.

4.4 Gas Chromatographic Analysis

The final products of decomposition reactions at different temperatures were identified by GC analysis. Cottrell et al. have previously reported the thermal decomposition products of nitroethane using infrared spectroscopy, showing approximately 8% CO_2, 45% NO, and 36% C_2H_4. However, the reaction temperature for these products was not included. In this work, GC experiments were conducted at different reaction temperatures, between 600 K and 1000 K. The decomposition products observed were essentially the same at all temperatures, although there were changes in the relative abundances of products at different temperatures. This GC analysis has made it possible to track the extent of decomposition for each reaction.

By comparing computed results to the GC experimental data, it is seen that the mechanism in Table 5.1 reproduces well the distributions of major products. The agreement between experiments and simulations is reasonably good, although some high molecular weight organic compounds were also found in the experiments.

There have been debates on the decomposition mechanism of nitroethane for a long time. Cottrell et al. found that the decomposition of nitroethane to be a first order reaction and proceeded with CEM mechanism. However, Gary and coworkers disputed this mechanism.[99] They found that products of HCHO, NO_2, CO_2, NO, C_2H_4, and C_2H_6 were generated in the decomposition products by the mass spectrometric method. They found the activation energy to be 39 kcal/mol and the decomposition is accomplished by the formation of radicals above 500 $^{\circ}$C. The formation of C_2H_4 was explained as the decomposition of radical C_2H_5. Wilde carried out an investigation of the decomposition

of nitroethane in flow and under static conditions.[100] It was shown that the main products were C_2H_4 and NO in the temperature range of 414–442 ˚C. The large amounts of C_2H_4 and low activation energy might be due to the elimination mechanism of HONO, while the formation of product such as HCHO, CH_4 and CO cannot be explained without reference to free radical processes.

Figure 5.9 shows both the simulation and experimental results of the ratio of C_2H_4 over NO at different temperatures. The symbols in the figures are experimental values and the solid lines are numerical simulations based on the proposed mechanism. It is clear that single mechanism cannot explain the decomposition behaviors and all three initial steps should be considered in the mechanism.

We suggest that concerted molecular elimination (CME) mechanism is the predominant path for the decompositions at low temperature (< 720±20 K). The dissociation of C–N bond becomes significantly for the decomposition at 720±20 K. Therefore, at temperature above 720±20 K the fraction of radical processes rises with the temperature.

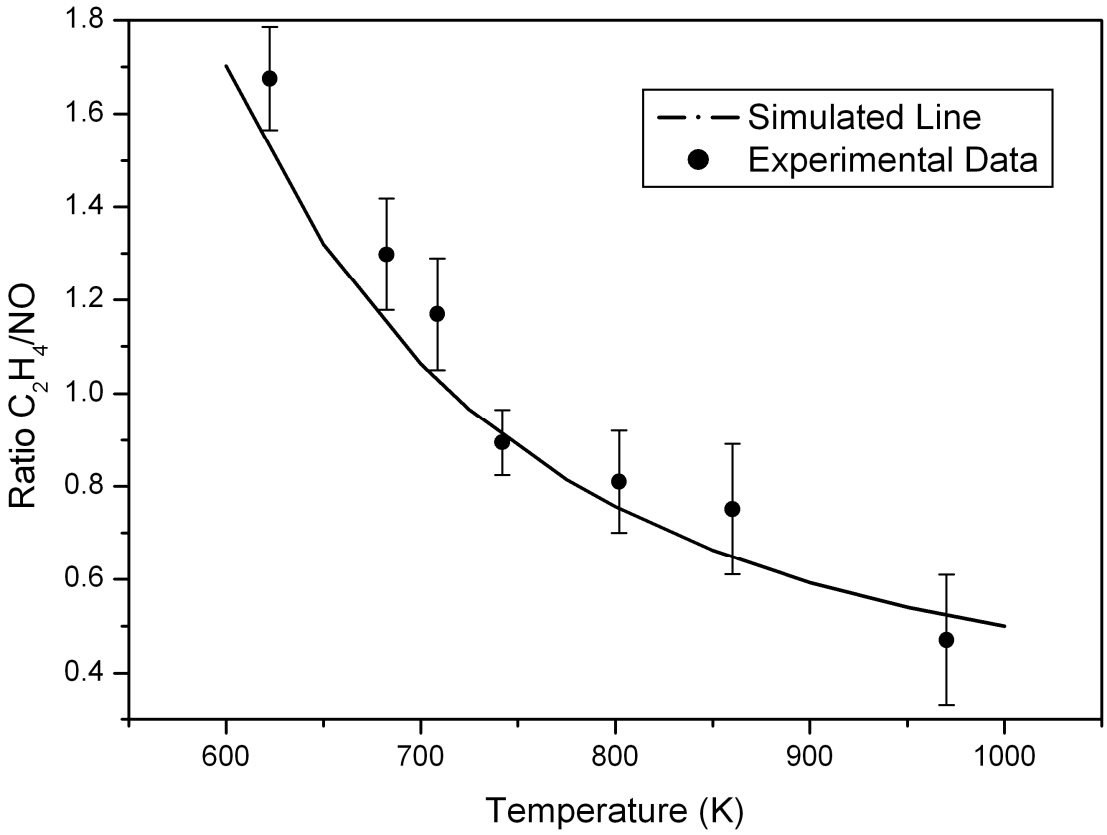

Figure 5.9 The concentration ratio of C_2H_4 to NO at different temperature. The symbols are experimental values and the solid line is based on numerical simulations, per the mechanism in Table 5.1.

It should be noted that no final product of N_2 was detected by GC experiments. There are extensive studies on a Selective Catalytic Reduction (SCR) process (also called $DeNO_x$) to remove nitrogen oxides (NO_x) or to form N_2.[101] Acid zeolites loaded with transition metals have been intensively investigated as catalysts for selective catalytic reduction of NO_x using hydrocarbons.[102] The reaction mechanism developed in this work is only for the decomposition of pure nitroethane at high temperature; however, it may provide useful information for $DeNO_x$ research.

5. Conclusions

A systematic study was performed to investigate the thermal decomposition behavior of nitroethane in gas phase using theoretical and experimental tools. Arrhenius parameters of $A = 10^{13.5\pm0.2}$ and $E_a = 46.2\pm0.5$ kcal/mol were derived for the decomposition temperature of 270–388 °C, which gave a good fit to the experimental data. From the schematic potential energy surface, the concerted molecular elimination was found to be the most favorable pathway. However, nitro-nitrite isomerization and rupture of C–NO_2 cannot be neglected during the initial decomposition process. The full reaction mechanism was proposed following the initial reactions, and was numerically solved. The GC analysis also indicated that there is a good agreement between experiment and simulation results. It was concluded that the concerted molecular elimination was dominant at the temperature lower than 720±20 K while the rupture of C–NO_2 would play an important role when increasing the reaction temperature. The outcome of this work is useful to understand the essential thermal properties and kinetics of nitro compounds.

CHAPTER VI

THERMAL RISK ASSESSMENT *

1. Background

Thermal risk evaluation of reaction hazards is of great importance to the safer operation of chemical processes. The thermal reactivity or thermal instability of a compound is an inherent property of the compound and the characterization of the thermal reactivity is considered as a dynamic problem.[103]

Both thermodynamic and kinetic studies are necessary to evaluate the thermal risk. In previous research by Ando *et al.*,[104] the onset temperature (T_o) and the heat of reaction ($-\Delta H_r$) are considered as two significant parameters to assess reaction hazards. It was suggested that thermal risk of chemical reactions could be characterized both by their severity and by their probability. First, the severity of a chemical reaction has to be determined. Usually severity can be described by the heat of reaction or the adiabatic temperature rise.[105] If the process temperature is above the onset temperature, the time to maximum rate under adiabatic condition (TMR_{ad}) could be used to describe the probability of thermal risk.[106]

---

* This chapter contains material reprinted with permission from Springer. Wang, Q.; Rogers, W. J.; Mannan, M. S. Thermal Risk Assessment and Rankings for Reaction Hazards in Process Safety. *J. Therm. Anal. Cal.* **2009**, *98*, 225–233.

It is well known that to evaluate the thermal reactivity and to design a safe chemical process, all the thermodynamic and kinetic parameters, including onset temperature, adiabatic time to maximum rate and maximum adiabatic temperature must be determined. But a correct determination of the thermo-chemical kinetics for a reaction is time consuming and therefore, preliminary screening methods, such as the Differential Scanning Calorimetry (DSC), are usually applied in the chemical industry. DSC is regarded as a useful screening tool for thermal risk assessment and for the investigation of decomposition mechanisms of exothermic reactions.[107]

The purpose of this chapter is to demonstrate that a reasonable ranking of thermal risk is possible. The demonstration is based on a kinetic model and correlations between T_o and E_a, and between T_o and TMR_{ad}, which are derived from a limited number, 37 sets, of DSC data. A new approach for assessing reaction hazards was also proposed and compared with a previous evaluation method of reaction hazards. We believe that the proposed ranking method of reaction hazards can be used to screen reaction hazards during chemical process designs.

2. Data Collection

Exothermic onset temperatures (T_o) and heats of reaction ($-\Delta H_r$) were collected from a previously published measurements in a pressure DSC (DU Pont 910 pressure-type). These experiments were performed with about 1-2 mg samples in an aluminum cell and a scanning rate of 10 °C/min for 820 reactive hazards of which 37 reactive hazards were chosen in this work. The data sets were selected on the basis of different

functional groups for compounds undergo decomposition with a bond scission as the first reaction step. The decomposition of these types of compounds may be first order, which will help to obtain a reasonable model later.

The concerned physical properties, such as molecular weight (MW) and specific heat capacity (C_p), are available from the National Institute of Standards and Technology. For those experimental values that are unavailable in the literature or handbooks, Gaussian03 programs were used to estimate them with good accuracy. Specific heat capacity values (J/K·mol) were calculated using the quicker and less expensive semi-empirical AM1 method. Both experimental and calculated data are displayed in Table 6.1.

Table 6.1. DSC data and physical property values for various compounds.

Compound name	Molecular formula	Molecular weight (g/mol)	Heat capacity (J/K·mol)	Heat of reaction (cal/g)	Onset temperature (°C)
Organic peroxides					
benzoyl peroxide	$C_{14}H_{10}O_4$	242	243	438	108
t-butyl hydroperoxide	$C_4H_{10}O_2$	90	123	252	98
cumene hydroperoxide	$C_9H_{12}O_2$	152	169	448	187
dilauroyl peroxide	$C_{24}H_{46}O_4$	399	387	232	86
di-tert-butyl peroxide (DTBP)	$C_8H_{18}O_2$	146	219	133	162
methylethylketone peroxide	$C_8H_{18}O_6$	210	220	345	99
Nitro compounds					
nitrobenzene	$C_6H_5NO_2$	123	186*	312	400
2,4,6-trinitrotoluene	$C_7H_5N_3O_6$	227	243*	1287	314
2-nitroaniline	$C_6H_6N_2O_2$	138	166*	485	341
3-nitroaniline	$C_6H_6N_2O_2$	138	159*	605	345
4-nitroaniline	$C_6H_6N_2O_2$	138	167*	601	347
2-nitrotoluene	$C_7H_7NO_2$	137	172*	317	338
3-nitrotoluene	$C_7H_7NO_2$	137	172*	260	361
4-nitrotoluene	$C_7H_7NO_2$	137	172*	372	366

Table 6.1. Continued

Compound name	Molecular formula	Molecular weight (g/mol)	Heat capacity (J/K·mol)	Heat of reaction (cal/g)	Onset temperature (°C)
Oximes					
benzaldoxime	C_7H_7NO	121	126	410	236
biacetylmonoxime	$C_4H_7NO_2$	101	122	220	159
cyclohexanoneoxime	$C_6H_{11}NO$	113	199*	527	207
dimethylglyoxime	$C_4H_8N_2O_2$	116	142	455	254
Azo compounds					
azobenzene	$C_{12}H_{10}N_2$	182	229*	191	321
azoxybenzene	$C_{12}H_{10}N_2O$	198	185	405	307
Epoxy compounds					
2,3-epoxy-1-propanol	$C_3H_6O_2$	74	83	241	197
1,2-epoxypropane	C_3H_6O	58	125*	67	160
Chlorides					
benzoyl chloride	C_7H_5ClO	141	187*	481	190
benzyl chloride	C_7H_7Cl	127	182	269	172
o-chlorobenzoyl chloride	$C_7H_4Cl_2O$	175	125	865	164
2-amino-4-chlorophenol	C_6H_6NClO	144	134	48	164
2,6-dichlorobenzoyl chloride	$C_7H_3Cl_3O$	209	140	694	229
2,4,5-trichlorophenol	$C_6H_3Cl_3O$	197	141	699	268
1,3-dichloropropane	$C_3H_6Cl_2$	113	125*	81	243
N-oxides					
pyridine-N-oxide	C_5H_5NO	95	88	380	288
γ-picoline-N-oxide	C_6H_7NO	109	113	368	285
picolinic acid N-oxide	$C_6H_5NO_3$	139	130	307	224
trimethylamine N-oxide	$C_3H_{12}NO$	75	98	213	202
Hydrazine					
benzoylhydrazine	$C_7H_8N_2O$	136	144	259	260
1,2-diformylhydrazine	$C_2H_4N_2O_2$	88	99*	304	234
2-hydroxyethylhydrazine	$C_2H_8N_2O$	76	95	251	240
4-nitrophenylhydrazine	$C_6H_7N_3O_2$	153	151	432	178

* Heat capacity data are from the open literature, other heat capacity data are calculated by Gaussian03 programs.

3. Model Development

In order to relate calorimetric data (T_o, $-\Delta H_r$) to activation energy and time to maximum rate, an unsteady state model in an adiabatic batch reactor was employed.[108] It has been shown that such a model can fairly well relate calorimetric data with activation energy and is based on the following assumptions:[109]

- The reaction system is assumed to be adiabatic, and therefore heat losses are negligible.
- The mass and volume of the liquid phase remain constant (i.e. evaporation losses are neglected). The specific heat of the liquid is considered to be constant during the reaction.
- A uniform temperature exists throughout the liquid phase.
- The decomposition reaction is first order with concentration, therefore

$$r_A = kC_A \tag{6.1}$$

With these assumptions, the following heat balance can be written

$$(-\Delta H_r)(-r_A)V + \Phi m C_p \frac{dT}{dt} = 0 \tag{6.2}$$

where ΔH_r is the heat of reaction (kJ/mol), r_A is the reaction rate (mol/m^3·s), V is the reaction volume (m^3), m and C_p are the mass (kg) and specific heat capacity (J/kg·K) of the chemical compound, respectively. Φ is the thermal inertia coefficient which is defined as

$$\Phi = \frac{mC_p + m_c C_{pc}}{mC_p} \tag{6.3}$$

where m_c and C_{pc} correspond to the mass (kg) and specific heat of the container (J/kg·K). The thermal inertia coefficient is one of the most important parameters to insure that the calorimeter matches as close as possible to the chemical process.

For typical industrial reactors, Φ is larger than but close to 1. However, to simplify the kinetic model, $\Phi = 1$ will be chosen in this work, which is the worse case for a thermal runaway reaction. In this case of $\Phi = 1$, all of the thermal energy released by the decomposition reaction will increase the temperature of the reacting system and accelerate the reaction. Combining equations 6.1 and 6.2

$$\frac{dT}{dt} = \frac{-\Delta H_r k C_A V}{\Phi m C_p} \tag{6.4}$$

with $C_p^{'} = (m/C_A V)C_p$ ($C_p^{'}$ is specific heat of the sample in J/mol·K) and $\Phi = 1$, equation 6.4 can be simplified as

$$\frac{dT}{dt} = \frac{-\Delta H_r k}{C_p^{'}} \tag{6.5}$$

According to Transition State Theory (TST), the rate constant k can be represented by

$$k = \frac{k_B T}{h} \exp(-\frac{E_a}{RT}) \tag{6.6}$$

where k_B is the Boltzmann's factor (J/K), h is Planck's constant (J·s), E_a is the activation energy (kJ/mol), T is the absolute temperature (K) and R is the gas constant (J/mol·K). Substituting equation 6.6 into 6.5

$$\frac{dT}{dt} = \frac{-\Delta H_r k_B T}{C_p^{'} h} \exp(-\frac{E_a}{RT}) \tag{6.7}$$

If the temperature at which the gradient of temperature with time (dT/dt) increases at the specified rate of 0.1 °C/min is taken as the onset temperature, activation energy can be calculated from equation 6.7.

For a decomposition reaction with relative high activation energy, it has been shown that the adiabatic time to maximum rate (TMR_{ad}) can be approximated.[110]

$$TMR_{ad} = \frac{C_p RT^2}{\dot{q} E_a} \tag{6.8}$$

where $\dot{q}$ is the corresponding heat release rate (W/kg) at the temperature T, E_a is the activation energy (kJ/mol), and C_p is the specific heat of the reaction mass (J/kg·K). In this model the concentration decrease is neglected, so that the calculated TMR_{ad} is always shorter than the true adiabatic value and, thus, the difference is on the conservative side. The heat release rate is defined as

$$\dot{q} = (-\Delta H_r)(r_A V) \tag{6.9}$$

It is also possible to estimate the heat release rate at any temperature T

$$\dot{q} = \dot{q}_o \exp\left(\frac{E_a}{R}\left(\frac{1}{T_o} - \frac{1}{T}\right)\right) \tag{6.10}$$

where $\dot{q}_o$ is the heat release rate (W/kg) at the onset temperature T_o. Therefore, the adiabatic time to maximum rate starting from the onset temperature can be estimated as

$$TMR_{ad} = \frac{C_p RT_o^2}{\dot{q}_o E_a} \tag{6.11}$$

Combining equations 6.2, 6.9 and 6.10, the heat release rate is

$$\dot{q}_o = \frac{dT}{dt} C_p \tag{6.12}$$

Substituting equation 6.12 into 6.11

$$TMR_{ad} = \frac{RT_o^2}{(dT/dt)E_a} \tag{6.13}$$

For an onset temperature corresponding to dT/dt = 0.1 °C/min, the adiabatic time to maximum rate can be estimated from the onset temperature and the activation energy according to equation 6.13. It should be noted that the thermo-kinetic analysis mentioned above is at best approximate (especially for the calculation of TMR_{ad}). Therefore, the models do not apply in cases of multiple reactions (in a competitive consecutive reaction network) or catalysis reactions.

4. Results and Discussion

4.1 Correlations

As pointed out above, if the temperature at dT/dt = 0.1 °C/min is taken as the onset temperature, both the activation energy and the adiabatic time to maximum rate can be estimated using equations 6.7 and 6.13. All data of onset temperature, activation energy, and adiabatic time to maximum rate are summarized in Table 6.2.

Table 6.2. Summary of adiabatic time to maximum rate and activation energy.

Compound name	Heat of reaction (cal/g)	Onset temperature (°C)	Adiabatic time to maximum rate (min)	Activation energy (kJ/mol)
benzoyl peroxide	438	108	83	145
t-butyl hydroperoxide	252	98	82	139
cumene hydroperoxide	448	187	100	176
dilauroyl peroxide	232	86	79	135
di-tert-butyl peroxide	133	162	98	161
methylethylketone peroxide	345	99	82	141
nitrobenzene	312	400	147	256
2,4,6-trinitrotoluene	1287	314	124	231
2-nitroaniline	485	341	133	236
3-nitroaniline	605	345	133	239
4-nitroaniline	601	347	133	240
2-nitrotoluene	317	338	133	233
3-nitrotoluene	260	361	139	241
4-nitrotoluene	372	366	139	245
benzaldoxime	410	236	110	195
biacetylmonoxime	220	159	96	162
cyclohexanoneoxime	527	207	105	183
dimethylglyoxime	455	254	114	202
azobenzene	191	321	131	224
azoxybenzene	405	307	125	223
2,3-epoxy-1-propanol	241	197	103	177
1,2-epoxypropane	67	160	100	156
benzoyl chloride	481	190	101	177
benzyl chloride	269	172	98	167
o-chlorobenzoyl chloride	865	164	93	171
2-amino-4-chlorophenol	48	164	100	160
2,6-dichlorobenzoyl chloride	694	229	107	196
2,4,5-trichlorophenol	699	268	115	212
1,3-dichloropropane	81	243	116	191
pyridine-N-oxide	380	288	121	216
γ-picoline-N-oxide	368	285	121	214
picolinic acid N-oxide	307	224	108	190
trimethylamine N-oxide	213	202	105	178
benzoylhydrazine	259	260	117	202
1,2-diformylhydrazine	304	234	111	193
2-hydroxyethylhydrazine	251	240	113	194
4-nitrophenylhydrazine	432	178	98	173

Two correlations in equations 6.14 and 6.15 were developed based on the training set of 37 reaction hazards. Equation 6.14 shows the correlation between the onset temperature and the activation energy with an R^2 value of 0.99. Figure 6.1 displays the onset temperature against the activation energy.

$$T_o = 2.4953E_a - 247.7 \tag{6.14}$$

The second correlation was based on the adiabatic time to maximum rate and the onset temperature, as shown below as equation 6.15

$$TMR_{ad} = 0.2088T_o + 61.885 \tag{6.15}$$

This correlation also has an R^2 value of 0.99. The detailed information of the time to maximum rate against the onset temperature is displayed in Figure 6.2. These equations and figures indicate that three thermo-kinetic parameters, T_o, E_a, and TMR_{ad}, are closely related to each other.

The onset temperature can be approximately described as proportional to the activation energy. The adiabatic time to maximum rate is also proportional to the onset temperature. Therefore, a specific reaction hazard with high activation energy in the decomposition reaction will have relatively high onset temperature and the adiabatic time to maximum rate will be large, which means that the thermal risk of this reaction hazard is relatively lower.

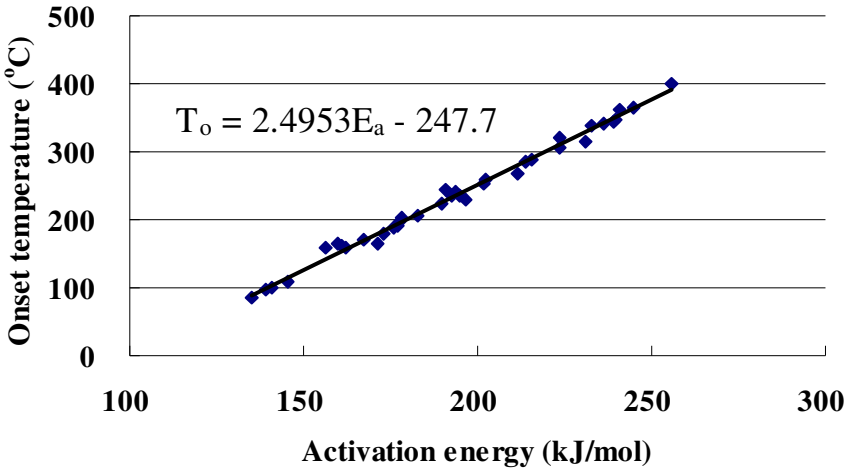

Figure 6.1. A correlation between onset temperature and activation energy.

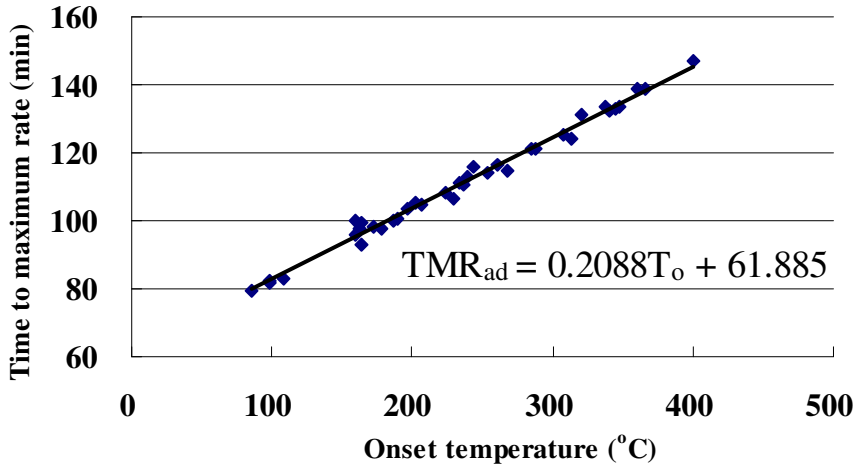

Figure 6.2. A correlation between adiabatic time to maximum rate and onset temperature.

According to equations 6.14 and 6.15, if the activation energy is known or can be estimated, then the onset temperature and the adiabatic time to maximum rate can be estimated. It is possible that the activation energy be estimated based on certain assumptions:

- The reaction follows a radical mechanism.
- The first step is the dissociation of the weakest bond, and the remaining steps are relatively fast.

Thermal decomposition reactions of the nitro compounds[111] or organic peroxides[112] can be depicted as bond scission reactions.

$$\text{R-NO}_2 \longrightarrow \text{R}\bullet + \text{NO}_2\bullet \qquad (6.16)$$

$$\text{RO-OR'} \longrightarrow \text{RO}\bullet + \text{R'O}\bullet \qquad (6.17)$$

Therefore, for these types of decomposition reactions (or any similar decomposition behaviors that have weakest bond broken), the bond scission reaction can be regarded as the rate-limiting step, and hence the activation energy can be estimated as:

$$E_a = \gamma_p\,(\text{BDE}) \qquad (6.18)$$

where γ_p is the positive transfer coefficient, BDE is the bond dissociation energy (kcal/mol) in the bond scission reaction, which can be calculated by Gaussian03 programs. The BDE data for some nitro compounds were collected from the published article by Saraf *et al*., and shown in Table 6.3. The experimental activation energy of dicumyl peroxide,[113] hydroxylamine,[114] and *t*-butyl peroxy acetate (TBPA)[115] were obtained from the previous literature. The onset temperatures are then predicted according to equation 6.14. As seen from Table 6.3, the average error percentages are

very small, and we can conclude that the predictions are reasonable and can be used to assess reaction hazards. The next section of this paper will show the thermal risk assessment of reaction hazards in detail.

Table 6.3. Summary of experimental and predicted values of onset temperature.

Compound	Bond dissociate energy (kcal/mol)	Predicted activation energy (kJ/mol)	Onset temperature (°C)	Predicted onset temperature (°C)	Error (%)
2-nitrotoluene	73.4	215	290	289	-0.4
3-nitrotoluene	75.9	222	310	307	-1.0
4-nitrotoluene	76.7	225	320	313	-2.2
2-nitrobenzoic acid	66.4	194	270	238	-12.0
3-nitrobenzoic acid	74.7	219	300	298	-0.6
4-nitrobenzoic acid	76.5	224	310	311	0.4
2-nitroaniline	80.1	235	280	338	20.6
3-nitroaniline	76.5	224	300	311	3.8
4-nitroaniline	80.9	237	310	344	10.8
dicumyl peroxide	—	147*	109	119	9.3
hydroxylamine	—	160*	139	152	9.0
TBPA	—	163*	160	159	-0.6

* Experimental values are from the previous literature.

4.2 Thermal Risk Evaluation

As we mentioned above, thermal risk is based on severity and probability. If these two parameters can be represented for a certain reaction hazard of chemical processes, thermal risk assessment of the reaction hazard is possible.

The primary factors determining severities in chemical reactions are the energies that can be released in the reactions based on quantities of chemicals and the adiabatic temperature rise potentials. Typical decomposition thermal energies can lead to massive destruction even if they are only partially transformed into mechanical forms in a thermal runaway incident. Secondary effects, such as the release of toxic compounds, can significantly contribute to the overall degree of the severity. However, in this work we will not focus on toxic effects. Therefore, the heat of reaction, which is a measure of the energy release potential of a compound, will be used as a measure of the severity of the reaction.

Probabilities of thermal runaway reactions are more difficult to evaluate. However, it is reasonable to consider their immediate consequences by referring to time scales of runaway scenarios, or the adiabatic time to maximum rate starting from the onset temperature. It is obviously that a failure mode that triggers a severe runaway reaction within a few minutes following the onset temperature is dangerous. Therefore, the adiabatic time to maximum rate will be used to represent the probability of runaway reaction occurrence.

4.2.1 Thermal Risk Index (TRI)

In order to assess quantitatively a specific reactive hazard, it is necessary to define two parameters related to severity and probability. Di-tert-butyl peroxide (DTBP) is an extensively studied chemical[116] for its thermally unstable and simple unimolecular first-order decomposition reaction in the gas phase. Therefore, DTBP is selected in this work as a reference compound to standardize the thermal risk index.

The heat of reaction, $-\Delta H_r$ = 133 cal/g, and the adiabatic time to maximum rate, TMR_{ad} = 98 min, for DTBP is used to define two dimensionless parameters and then estimate thermal reactivity risk. A ratio, β, as the amount of energy released by a specific substance to the energy released by DTBP is defined

$$\beta = \frac{-\Delta H_r}{133} \tag{6.19}$$

β is measurement of the severity of the reaction. The higher the value of β, more severe the chemical reaction is relative to the decomposition reaction of DTBP.

We can also define another ratio, ε, as the adiabatic time to maximum rate of DTBP to that of the substance.

$$\varepsilon = \frac{98}{TMR_{ad}} \tag{6.20}$$

ε is measurement of probability of reaction occurrence. The smaller the value of ε, the safer the process is, because there is more time to make adjustments to avert a runaway reaction or to reduce the consequences.

Because risk is the function of severity and probability, it may be expressed by these two parameters (although there are some other factors that may contribute to the risk):

$$\text{Risk} = \text{Severity} \times \text{Probability} \tag{6.21}$$

Combining definitions (19), (20), and (21), the thermal risk of a specific substance relative to DTBP can be represented quantitatively by defining a thermal risk index (TRI) as follows

$$TRI = \beta \times \varepsilon = \left(\frac{-\Delta H_r}{133} \right) \times \left(\frac{98}{TMR_{ad}} \right) \tag{6.22}$$

Table 6.4. Results of TRI and RHI rankings.

Compound name	Thermal risk index		Reaction hazard index		Overall ranking
	TRI value	Ranking	RHI value	Ranking	
benzoyl peroxide	3.89	4	6.79	4	High
t-butyl hydroperoxide	2.25	3	5.35	3	Medium
cumene hydroperoxide	3.30	4	6.30	4	High
dilauroyl peroxide	2.15	3	5.84	3	Medium
di-tert-butyl peroxide	1.00	2	4.12	2	Medium
methylethylketone peroxide	3.12	4	6.34	4	High
nitrobenzene	1.56	2	4.56	2	Medium
2,4,6-trinitrotoluene	7.65	4	7.72	4	High
2-nitroaniline	2.70	3	5.76	3	Medium
3-nitroaniline	3.36	4	6.22	4	High
4-nitroaniline	3.32	4	6.11	4	High
2-nitrotoluene	1.75	2	5.00	2	Medium
3-nitrotoluene	1.38	2	4.65	2	Medium
4-nitrotoluene	1.97	2	5.17	3	Medium
benzaldoxime	2.74	3	6.07	4	High
biacetylmonoxime	1.69	2	5.07	3	Medium
cyclohexanoneoxime	3.70	4	5.69	3	High
dimethylglyoxime	2.93	3	5.90	3	Medium
azobenzene	1.07	2	4.34	2	Medium
azoxybenzene	2.38	3	5.99	3	Medium
2,3-epoxy-1-propanol	1.72	2	5.18	3	Medium
1,2-epoxypropane	0.49	1	3.35	1	Low
benzoyl chloride	3.52	4	6.10	4	High
benzyl chloride	2.01	3	5.06	3	Medium
o-chlorobenzoyl chloride	6.87	4	8.18	4	High
2-amino-4-chlorophenol	0.36	1	3.63	1	Low
2,6-dichlorobenzoyl chloride	4.79	4	7.75	4	High
2,4,5-trichlorophenol	4.48	4	7.53	4	High
1,3-dichloropropane	0.51	1	3.76	1	Low
pyridine-N-oxide	2.31	3	5.96	3	Medium
γ-picoline-N-oxide	2.24	3	5.71	3	Medium
picolinic acid N-oxide	2.09	3	5.79	3	Medium
trimethylamine N-oxide	1.49	2	4.75	2	Medium
benzoylhydrazine	1.64	2	5.18	3	Medium
1,2-diformylhydrazine	2.02	3	5.42	3	Medium
2-hydroxyethylhydrazine	1.64	2	4.93	2	Medium
4-nitrophenylhydrazine	3.25	4	6.48	4	High

The lower the value of TRI, the lower the thermal risk is due to a lower reactivity. The thermal risk index values for all 37 compounds are calculated according to equation 6.22 and shown in Table 6.4. In this work, we assign thermal risk ranking values according to the rules as follows:

1 for TRI < 1;

2 for 1 ≤ TRI <2;

3 for 2 ≤ TRI <3;

4 for TRI ≥ 3

Therefore, thermal risk rankings for all 37 reaction hazards are assigned and summarized in Table 6.4.

4.2.2 Reaction Hazard Index (RHI)

D. R. Stull has developed a ranking system, which is called the reaction hazard index (RHI), to establish the relative potential hazards of specific reactive chemicals.[117] The RHI relates the maximum adiabatic temperature (T_m) to the activation energy (E_a) of a decomposition reaction and is defined as

$$RHI = \frac{10T_m}{T_m + 30E_a} \tag{6.23}$$

where E_a is the activation energy (kcal/mol), and T_m is the maximum adiabatic decomposition temperature (K), which can be estimate as

$$T_m = T_o + \frac{-\Delta H_r}{C_p'} \tag{6.24}$$

where T_o is the onset temperature (K), $C_p^{'}$ is the specific heat of the sample (J/mol·K), and ΔH_r is the heat of reaction (kJ/mol).

The reaction hazard index values for all 37 reaction hazards are calculated and included in Table 6.4. The reaction hazard index relationship has a low value (RHI < 4) for relative low reactivity and high value (RHI > 6) for high reactivity. In this work, RHI rankings are assigned according to the rules as follows:

1 for RHI < 4;

2 for 4 ≤ RHI <5;

3 for 5 ≤ RHI <6;

4 for RHI ≥ 6

Based on two ranking methods (TRI and RHI), overall rankings in low, medium and high are also provided in Table 6.4. The methods of TRI and RHI are consistent with each other and are useful for the preliminary thermal risk assessment of reaction hazards. However, we would like to stress here that the methods of TRI and RHI are only for giving a general and global classification, and experimental tests are necessary to obtain the further accurate information of chemical reactivity.

5. Conclusions

The thermal reaction hazards can be evaluated through the aid of calorimetry with related models. In this work, the kinetic model under adiabatic conditions for the first order reaction was developed and two simple correlations among onset temperature, adiabatic time to maximum rate, and activation energy were presented. The correlations

relate the main characteristics of the decomposition reactions with acceptable accuracy. If the activation energy is known or can be estimated, the onset temperature and the adiabatic time to maximum rate can be estimated. Both the heat of reaction and the adiabatic time to maximum rate can then be used to evaluate potential reaction hazards.

To represent the thermal risk for a chemical substance, a method of thermal risk index (TRI) was defined by product of severity and probability relative to DTBP. Reaction hazard index (RHI) values were also calculated based on activation energy and maximum adiabatic temperature. The final ranking results of these two methods are consistent with each other. The analysis presented in this work has potential applications in process safety, loss prevention, and emergency response for thermally sensitive hazards.

CHAPTER VII

CONCLUSIONS

Evaluation of chemical reactivity in the chemical industry has attracted attentions of lots of researchers in the last few decades in anticipation of possible regulations. This work is intended to resolve some of the current runaway incident cases and advance reactive hazard assessment. Advanced methods of reactivity evaluation are primarily thermal analysis techniques and theoretical calculations or prediction, which are capable of providing overall thermodynamic and kinetic description.

In this work, a combination of computational quantum chemistry methods, thermodynamic-energy correlations, and experimental analysis resulted in a better understanding of several reactive chemical systems. Methylcyclopentadiene (unsaturated hydrocarbons), hydroxylamine, and energetic materials systems have been successfully evaluated. The primary reaction pathways, reaction mechanisms and their thermodynamic/kinetic parameters have been determined as well.

Computation quantum chemistry calculations together with experimental analysis focus on the most possible and most hazardous reactions. These detailed and advanced analyses should be required for more complex reactive systems.

A thermal risk assessment or index based on TMR and $-\Delta H$, which can be obtained from calorimetric data or theoretical methods, was proposed to help recognize the more hazardous compositions. Some correlations to predict onset temperature and TMR using molecular modeling were explored. This method of thermal risk assessment

has significantly improved screening potential for identifying reaction hazards. When these findings were compared to the literature information, a great level of agreement and consistency existed.

The area of reactive chemicals is still presenting unique challenges and this work has demonstrated that the application of theoretical and experimental levels of evaluation should be conducted in parallel to enhance the understanding of reaction chemistry. In this work, the focus was on evaluating single reactive systems. However, the work could be extended to mixtures of reactive systems based on the same principles of theoretical computational chemistry and experimental analysis.

REFERENCES

1. *Improving Reactive Hazard Management*; Report of U.S. Chemical Safety and Hazard Investigation Board Hazard Investigation: Washington DC, 2002.
2. Saraf, S. R.; Rogers, W. J.; Mannan, M. S. Using Screening Test Data to Recognize Reactive Chemical Hazards. *Journal of Hazardous Materials* **2003**, *104* (1-3), 255-267.
3. Bretherick, L. *Reactive Chemical Hazards: An Overview*; AIChE: New York, 1987.
4. Heemskerk, A. H.; Hordijk, A. C.; Lanning, A. T.; Lont, J. C.; Schell, H.; Schuurman, P. *Guidelines for Chemical Reactivity Evaluation and Application to Process Design*; AIChE: New York, 1995.
5. Duh, Y. S.; Wu, X. H.; Kao, C. S. Hazard Ratings for Organic Peroxides. *Process Safety Progress* **2008**, *27* (2), 89-99.
6. Hou, H. Y.; Shu, C. M.; Duh, Y. S. Exothermic Decomposition of Cumene Hydroperoxide at Low Temperature Conditions. *AIChE Journal* **2001**, *47* (8), 1893-1896.
7. Voloshin, Y.; Manganaro, J.; Lawal, A. Kinetics and Mechanism of Decomposition of Hydrogen Peroxide over Pd/SiO_2 Catalyst. *Industrial & Engineering Chemistry Research* **2008**, *47* (21), 8119-8125.
8. Saraf, S. R.; Rogers, W. J.; Mannan, M. S. Classifying Reactive Chemicals. *Chemical Engineering Progress* **2004**, *100* (3), 34-37.

9. Aldeeb, A. A. Systematic Approach for Chemical Reactivity Evaluation. Texas A&M University Doctoral Thesis, College Station, TX, 2003.

10. Foresman, J. B.; Frisch, A. *Exploring Chemistry with Electronic Structure Methods*. Second ed.; Gaussian, Inc.: Pittsburgh, PA, 1996.

11. Frisch, M. J.; Trucks, G. W.; Schlegel, H. B.; Scuseria, G. E.; Robb, M. A. et al. Official Gaussian Website; http://www.gaussian.com/g_prod/g09.htm: Wallingford, CT, 2010.

12. Becke, A. D. Density-Functional Thermochemistry 3: The Role of Exact Exchange. *Journal of Chemical Physics* **1993**, *98* (7), 5648-5652.

13. Lee, C. T.; Yang, W. T.; Parr, R. G. Development of the Colle-Salvetti Correlation-energy Formula into a Functional of the Electron-density. *Physical Review B* **1988**, *37* (2), 785-789.

14. Frisch, M. J.; Trucks, G. W.; Schlegel, H. B.; Scuseria, G. E.; Robb, M. A. et al. Official Gaussian Website; http://www.gaussian.com/index.htm: Wallingford, CT, 2010.

15. Barton, J.; Rogers, R. *Chemical Reaction Hazards: A Guide to Safety*. Second ed.; The Institution of Chemical Engineers: Rugby, UK, 1997.

16. Center for Chemical Process Safety, *Guidelines for Safe Storage and Handling of Reactive Materials*; AIChE: New York, 1995.

17. Saraf, S. R. Molecular Characterization of Energetic Materials. Texas A&M University Doctoral Thesis, College Station, TX, 2003.

18. Heldt, K.; Anderson, H. L. Application of an Adiabatic Calorimeter with Safety Concept. *Thermochimica Acta* **1996**, *271*, 189-194.

19. Wei, C. Y.; Rogers, W. J.; Mannan, M. S. Thermal Decomposition Hazard Evaluation of Hydroxylamine Nitrate. *Journal of Hazardous Materials* **2006**, *130* (1-2), 163-168.

20. U.S. Chemical Safety Board News Release, CSB Deploys to Fatal Jacksonville, Florida Explosion, December 19, 2007; http://www.csb.gov/newsroom/detail.aspx?nid=14

21. Wu, F. J.; Berris, B. C.; Bell, D. R. Process for Making Methylcyclopentadienyl Manganese Tricarbonyl Compounds; 1990, US Patent.

22. Saraf, S. R.; Rogers, W. J.; Mannan, M. S.; Hall, M. B.; Thomson, L. M. Theoretical Thermochemistry: Ab Initio Heat of Formation for Hydroxylamine. *Journal of Physical Chemistry A* **2003**, *107* (8), 1077-1081.

23. Csicsery, S. M. Methylcyclopentadiene Isomers. *Journal Organic Chemistry* **1960**, *25* (4), 518-521.

24. Ikeda, E.; Tranter, R. S.; Kiefer, J. H.; Kern, R. D.; Singh, H. J.; Zhang, Q. The Pyrolysis of Methylcyclopentadiene. *Proceedings of the Combustion Institute* **2000**, *28* (2), 1725-1732.

25. Dubnikova, F.; Lifshitz, A. Ring Expansion in Methylcyclopentadiene Radicals. *Journal of Physical Chemistry A* **2002**, *106* (35), 8173-8183.

26. Hehre, W. J.; Ditchfield, R.; Pople, J. A. Self-consistent Molecular-orbital Methods: 12. Future Extensions of Gaussian-type Basis Sets for Use in

Molecular-obital Studies of Organic-molecules. *Journal of Chemical Physics* **1972**, *56* (5), 2257-2261.

27. Spangler, C. W. Thermal [1,j] Sigmatropic Rearrangements. *Chemical Reviews* **1976**, *76* (2), 187-217.

28. Bachrach, S. M. Theoretical Studies of the [1,5] Sigmatropic Hydrogen Shift in Cyclopentadiene, Pyrrole, and Phosphole. *Journal of Organic Chemistry* **1993**, *58* (20), 5414-5421.

29. McLean, S.; Webster, C. J.; Rutherford, R. J. Kinetic Isotope Effect for the Thermally-induced Migration of Hydrogen in Cyclopentadienes. *Canadian Journal of Chemistry* **1969**, *47* (9), 1555-1559.

30. Woodward, R. B.; Katz, T. J. The Mechanism of the Diels-Alder Reaction. *Tetrahedron* **1959**, *5* (1), 70-89.

31. Froese, R. D. J.; Organ, M. G.; Goddard, J. D.; Stack, T. D. P.; Trost, B. M. Theoretical and Experimental Studies of the Diels-Alder Dimerizations of Substituted Cyclopentadienes. *Journal of the American Chemical Society* **1995**, *117* (44), 10931-10938.

32. Masel, R. I. *Chemical Kinetics and Catalysis*; John Wiley & Sons, Inc.: New York, 2001.

33. Diez, M. A.; Guillen, M. D.; Blanco, C. G.; Bermejo, J. Chromatographic Study of Methylcyclopentadiene Dimers and Iso-dimers and Determination of Their Boiling Points. *Journal of Chromatography* **1990**, *508* (2), 363-374.

34. Panda, T. K.; Gamer, M. T.; Roesky, P. W. An Improved Synthesis of Sodium and Potassium Cyclopentadienide. *Organometallics* **2003**, *22* (4), 877-878.

35. Hydroxylamine and Its Salts. *Manufacturing Chemist and Aerosol News* **1964**, *35* (8), 29-36.

36. Long, L. U.S. Chemical Safety and Hazard Investigation Board, The Explosion at Concept Sciences: Hazards of Hydroxylamine; Washington DC, 2002.

37. Reisch, M. Chemical Plant Blast Kills Five Near Allentown. *Chemical & Engineering News* **1999**, *77* (9), 11-12.

38. Business Concentrates, Chemical Explosion in Japan Kills Four. *Chemical & Engineering News* **2000**, *78* (25), 15-16.

39. Wei, C.; Saraf, S. R.; Rogers, W. J.; Mannan, M. S. Thermal Runaway Reaction Hazards and Mechanisms of Hydroxylamine with Acid/base Contaminants. *Thermochimica Acta* **2004**, *421* (1-2), 1-9.

40. Iwata, Y.; Koseki, H. Decomposition of Hydroxylamine/water Solution with Added Iron Ion. *Journal of Hazardous Materials* **2003**, *104* (1-3), 39-49.

41. Cisneros, L. O.; Wu, X.; Rogers, W. J.; Mannan, M. S.; Park, J.; North, S. W. Decomposition Products of 50 Mass% Hydroxylamine/water Under Runaway Reaction Conditions. *Process Safety and Environmental Protection* **2003**, *81* (B2), 121-124.

42. Cisneros, L. O.; Rogers, W. J.; Mannan, M. S.; Li, X.; Koseki, H. Effect of Iron Ion in the Thermal Decomposition of 50 Mass % Hydroxylamine/water Solutions. *Journal of Chemical & Engineering Data* **2003**, *48* (5), 1164-1169.

43. Cisneros, L. O.; Rogers, W. J.; Mannan, M. S. Effect of Air in the Thermal Decomposition of 50 Mass% Hydroxylamine/water. *Journal of Hazardous Materials* **2002**, *95* (1-2), 13-25.

44. Cisneros, L. O.; Rogers, W. J.; Mannan, M. S. Adiabatic Calorimetric Decomposition Studies of 50 wt.% Hydroxylamine/water. *Journal of Hazardous Materials* **2001**, *82* (1), 13-24.

45. Hofmann, K. A.; Kroll, F. Thermal Decomposition of Hydroxylamine and Hydrazine Salts. *Berichte* **1924**, *57* (B), 937-944.

46. Nast, R.; Foppl, I. The Formation of Hyponitrite by the Disproportionation of Hydroxylamine. *Zeitschrift für anorganische und allgemeine Chemie* **1950**, *263* (5-6), 310-315.

47. Lunak, S.; Veprek-Siska, J. The Catalytic Effect of Cations on the Decomposition of Alkaline Solutions of Hydroxylamine. *Collection of Czechoslovak Chemical Communications* **1972**, *39* (2), 391-395.

48. Holzapfel, H. Decomposition of Hydroxylamine in Strongly Alkaline, Aqueous Solutions. *Wissenschaftliche Zeitschrift - Karl-Marx-Universitaet Leipzig, Mathematisch-Naturwissenschaftliche Reihe* **1960**, *1959-1960* (9), 17-25.

49. Hughes, M. N.; Nicklin, H. G. Oxidation of Hydroxylamine by Molecular Oxygen in Alkaline Solutions. *Chemistry and Industry* **1967**, (52), 2176-2177.

50. Hughes, M. N.; Nicklin, H. G. Autoxidation of Hydroxylamine in Alkaline Solutions. *Journal of the Chemical Society A* **1971,** (1), 164-168.

51. Alluisetti, G. E.; Almaraz, A. E.; Amorebieta, V. T.; Doctorovich, F.; Olabe, J. A. Metal-catalyzed Anaerobic Disproportionation of Hydroxylamine. Role of Diazene and Nitroxyl Intermediates in the Formation of N_2, N_2O, NO^+, and NH_3. *Journal of the American Chemical Society* **2004,** *126* (41), 13432-13442.

52. Bengtsson, G.; Fronaus, S.; Bengtsson-Kloo, L. The Kinetics and Mechanism of Oxidation of Hydroxylamine by Iron (III). *Journal of the Chemical Society, Dalton Transactions* **2002**, (12), 2548-2552.

53. Frisch, M. J.; Trucks, G. W.; Schlegel, H. B.; Scuseria, G. E.; Robb, M. A.; Cheeseman, J. R.; J. A. Montgomery, J.; Vreven, T.; Kudin, K. N.; Burant, J. C.; Millam, J. M.; Iyengar, S. S.; Tomasi, J.; Barone, V.; Mennucci, B.; Cossi, M.; Scalmani, G.; Rega, N.; Petersson, G. A.; Nakatsuji, H.; Hada, M.; Ehara, M.; Toyota, K.; Fukuda, R.; Hasegawa, J.; Ishida, M.; Nakajima, T.; Honda, Y.; Kitao, O.; Nakai, H.; Klene, M.; Li, X.; Knox, J. E.; Hratchian, H. P.; Cross, J. B.; Adamo, C.; Jaramillo, J.; Gomperts, R.; Stratmann, R. E.; Yazyev, O.; Austin, A. J.; Cammi, R.; Pomelli, C.; Ochterski, J. W.; Ayala, P. Y.; Morokuma, K.; Voth, G. A.; Salvador, P.; Dannenberg, J. J.; Zakrzewski, V. G.; Dapprich, S.; Daniels, A. D.; Strain, M. C.; Farkas, O.; Malick, D. K.; Rabuck, A. D.; Raghavachari, K.; Foresman, J. B.; Ortiz, J. V.; Cui, Q.; Baboul, A. G.; Clifford, S.; Cioslowski, J.; Stefanov, B. B.; Liu, G.; Liashenko, A.; Piskorz, P.; Komaromi, I.; Martin, R. L.; Fox, D. J.; Keith, T.; Al-Laham, M. A.; Peng, C. Y.; Nanayakkara, A.; Challacombe, M.; Gill, P. M. W.; Johnson, B.; Chen, W.; Wong, M. W.;

Gonzalez, C.; Pople, J. A. Gaussian 03, Revision B.05; Gaussian, Inc.: Pittsburgh PA, 2003.

54. Becke, A. D. Density-functional Thermochemistry. III. The Role of Exact Exchange. *Journal of Chemical Physics* **1993,** *98* (7), 5648-5652.

55. Lee, C.; Yang, W.; Parr, R. G. Development of the Colle-Salvetti Correlation Energy Formula into a Functional of the Electron Density. *Physical Review B* **1988,** *37* (2), 785-789.

56. Lynch, B. J.; Fast, P. L.; Harris, M.; Truhlar, D. G. Adiabatic Connection for Kinetics. *Journal of Physical Chemistry A* **2000,** *104* (21), 4811-4815.

57. Dunning, T. H., Jr. Gaussian Basis Sets for Use in Correlated Molecular Calculations. I. The Atoms Boron through Neon and Hydrogen. *Journal of Chemical Physics* **1989,** *90* (2), 1007-1023.

58. Hehre, W. J.; Ditchfield, R.; Pople, J. A. Self-consistent Molecular Orbital Methods. XII. Further Extensions of Gaussian-type Basis Sets for Use in Molecular Orbital Studies of Organic Molecules. *Journal of Chemical Physics* **1972,** *56* (5), 2257-2261.

59. Clark, T.; Chandrasekhar, J.; Spitznagel, G. W. Efficient Diffuse Function-augmented Basis Sets for Anion Calculations. III. The 3-21+G Basis Set for First-row Elements, Lithium to Fluorine. *Journal of Computational Chemistry* **1983,** *4* (3), 294-301.

60. Frisch, M. J.; Pople, J. A.; Binkley, J. S. Self-consistent Molecular Orbital Methods. 25. Supplementary Functions for Gaussian Basis Sets. *Journal of Chemical Physics* **1984,** *80* (7), 3265-3269.

61. Li, Q. S.; Xu, X. D.; Zhang, S. Predicting Energies and Geometries for Reactions Involved in Atmosphere Chemistry: A Comparison Study between Hybrid DFT Methods. *Chemical Physics Letters* **2004,** *384* (1-3), 20-24.

62. Coote, M. L. Reliable Theoretical Procedures for the Calculation of Electronic-structure Information in Hydrogen Abstraction Reactions. *Journal of Physical Chemistry A* **2004,** *108* (17), 3865-3872.

63. Zhao, Y.; Lynch, B. J.; Truhlar, D. G. Development and Assessment of a New Hybrid Density Functional Model for Thermochemical Kinetics. *Journal of Physical Chemistry A* **2004,** *108* (14), 2715-1719.

64. Pople, J. A.; Head-Gordon, M.; Raghavachari, K. Quadratic Configuration Interaction: A General Technique for Determining Electron Correlation Energies. *Journal of Chemical Physics* **1987,** *87* (10), 5968-5975.

65. Head-Gordon, M.; Pople, J. A.; Frisch, M. J. MP2 Energy Evaluation by Direct Methods. *Chemical Physics Letters* **1988,** *153* (6), 503-506.

66. Petersson, G. A.; Bennett, A.; Tensfeldt, T. G.; Al-Laham, M. A.; Shirley, W. A.; Mantzaris, J. A Complete Basis Set Model Chemistry 1: The Total Energies of Closed-shell Atoms and Hydrides of the First-row Elements. *Journal of Chemical Physics* **1988,** *89* (4), 2193.

67. Gonzalez, C.; Schlegel, H. B. An Improved Algorithm for Reaction Path Following. *Journal of Chemical Physics* **1989,** *90* (4), 2154-2161.

68. Gonzalez, C.; Schlegel, H. B. Reaction Path Following in Mass-weighted Internal Coordinates. *Journal of Physical Chemistry* **1990,** *94* (14), 5523-5527.

69. Tsunekawa, S. Microwave Spectrum of Hydroxylamine. *Journal of Physical Society of Japan* **1972,** *33* (1), 167-174.

70. Tyrrell, J.; Lewis-Bevan, W.; Kristiansen, D. Equilibrium Geometries, Internal Rotation Potentials, and Spectroscopic Constants in NH_2OH, NH_2OF, NHFOH, and NHFOF. *Journal of Physical Chemistry* **1993,** *97* (49), 12768-12772.

71. Chung-Phillips, A.; Jebber, K. A. *Ab Initio* Studies of Critical Conformations in Ethane, Methylamine, Methanol, Hydrazine, Hydroxylamine, and Hydrogen Peroxide. *Journal of Chemical Physics* **1995,** *102* (18), 7080-7087.

72. Boulet, P.; Gilardoni, F.; Weber, J.; Chermette, H.; Ellinger, Y. Theoretical Study of Interstellar Hydroxylamine Chemistry: Protonation and Proton Transfer Mediated by H_3^+. *Chemical Physics* **1999**, *244* (2-3), 163-174.

73. Mahoney, L. R.; Mendenhall, G. D.; Ingold, K. U. Calorimetric and Equilibrium Studies on Some Stable Nitroxide and Iminoxy Radicals: Approximate O-H Bond Dissociation Energies in Hydroxylamines and Oximes. *Journal of the American Chemical Society* **1973**, *95* (26), 8610-8614.

74. Brönstrup, M.; Schröder, D.; Kretzschmar, I.; Schalley, C. A.; Schwarz, H. Mass-spectrometric Experiments Together with Electronic Structure Calculations

Support the Existence of the Elusive Ammonia Oxide Molecule and Its Radical Cation. *European Journal of Inorganic Chemistry* **1998**, *1998* (10), 1529-1538.

75. Barone, V.; Cossi, M. Quantum Calculation of Molecular Energies and Energy Gradients in Solution by a Conductor Solvent Model. *Journal of Physical Chemistry A* **1998**, *102* (11), 1995-2001.

76. Cossi, M.; Rega, N.; Scalmani, G.; Barone, V. Energies, Structures, and Electronic Properties of Molecules in Solution with the C-PCM Solvation Model. *Journal of Computational Chemistry* **2003**, *24* (6), 669-681.

77. Curtiss, L. A.; Raghavachari, K.; Trucks, G. W.; Pople, J. A. Gaussian-2 Theory for Molecular Energies of First- and Second-row Compounds. *Journal of Chemical Physics* **1991**, *94* (11), 7221-7230.

78. Agrawal, J. P.; Hodgson, R. D. *Organic Chemistry of Explosives*; Wiley: New York, 2007.

79. Brill, T. B.; Russell, T. P.; Tao, W. C.; Wardle, R. B. *Decomposition, Combustion, and Detonation Chemistry of Energetic Materials*; Materials Research Society: Pittsburgh, PA, 1996.

80. Shaw, R. W.; Brill, T. B.; Thompson, D. L. *Overviews of Recent Research on Energetic Materials*; World Scientific: Singapore, 2005.

81. Huang, K.; Wang, S. J. Design and Control of a Methyl Tertiary Butyl Ether (MTBE) Decomposition Reactive Distillation Column. *Industrial & Engineering Chemistry Research* **2007**, *46* (8), 2508–2519.

82. Prasad, V.; Vlachos, D. G. Multiscale Model and Informatics-Based Optimal Design of Experiments: Application to the Catalytic Decomposition of Ammonia on Ruthenium. *Industrial & Engineering Chemistry Research* **2008**, *47* (17), 6555-6567.

83. Wu, C. J.; Fried, L. E. Ab Initio Study of RDX Decomposition Mechanisms. *Journal of Physical Chemistry A* **1997**, *101* (46), 8675-8679.

84. Ju, X. H.; Xiao, H. M.; Xia, Q. Y. A Density Functional Theory Investigation of 1, 1-Diamino-2, 2-Dinitroethylene Dimers and Crystal. *Journal of Chemical Physics* **2003**, *119* (19), 10247-10255.

85. Alavi, S.; Reilly, L. M.; Thompson, D. L. Theoretical Predictions of the Decomposition Mechanism of 1, 3, 3-Trinitroazetidine (TNAZ). *Journal of Chemical Physics* **2003**, *119* (16), 8297-8304.

86. Taube, A. G.; Bartlett, R. J. Frozen Natural Orbital Coupled-cluster Theory: Forces and Application to Decomposition of Nitroethane. *Journal of Chemical Physics* **2008**, *128* (16), 164101-164117.

87. Benson, S. W.; Spokes, G. N. Very Low-pressure Pyrolysis I: Kinetic Studies of Homogeneous Reactions at the Molecular Level. *Journal of the American Chemical Society* **1967**, *89* (11), 2525-2532.

88. Benson, S. W.; O'Neal, H. E. *Kinetic Data on Gas Phase Unimolecular Reactions*; US Government Printing Office: Washington DC, 1970.

89. Shaw, R. Heats of Formation and Kinetics of Decomposition of Nitroalkanes. *International Journal of Chemical Kinetics* **2004**, *5* (2), 261-269.

90. Wodtke, A. M.; Hintsa, E. J.; Lee, Y. T. Infrared Multiphoton Dissociation of Three Nitroalkanes. *Journal of Physical Chemistry* **1986**, *90* (16), 3549-3558.

91. Denis, P. A.; Ventura, O. N.; Le, H. T.; Nguyen, M. T. Density Functional Study of the Decomposition Pathways of Nitroethane and 2-Nitropropane. *Physical Chemistry and Chemical Physics* **2003**, *5* (9), 1730-1738.

92. Hall, M. B.; Fenske, R. F. Electronic Structure and Bonding in Methyl-and perfluoromethyl (pentacarbonyl) Manganese. *Inorganic Chemistry* **1972**, *11* (4), 768-775.

93. Nazin, G. M.; Manelis, G. B. Thermal Decomposition of Aliphatic Nitro Compounds. *Russian Chemical Reviews* **1994**, *63* (4), 313-322.

94. Bhattacharya, A.; Guo, Y. Q.; Bernstein, E. R. Experimental and Theoretical Exploration of the Initial Steps in the Decomposition of a Model Nitramine Energetic Material: Dimethylnitramine. *Journal of Physical Chemistry A* **2009**, *113* (5), 811-823

95. Brill, T. B.; James, K. J. Kinetics and Mechanisms of Thermal Decomposition of Nitroaromatic Explosives. *Chemical Reviews* **1993**, *93* (8), 2667-2692.

96. Manaa, M. R.; Reed, E. J.; Fried, L. E.; Galli, G.; Gygi, F. Early Chemistry in Hot and Dense Nitromethane: Molecular Dynamics Simulations. *Journal of Chemical Physics* **2004**, *120* (21), 10146-10153.

97. Manaa, M. R.; Fried, L. E. DFT and Ab Initio Study of the Unimolecular Decomposition of the Lowest Singlet and Triplet States of Nitromethane. *Journal of Physical Chemistry A* **1998**, *102* (48), 9884-9889.

98. Mallard, W. G.; Westley, F.; Herron, J. T.; Hampson, R. F.; Frizzell, D. H. NIST Chemical Kinetics Database, Version 6.0.; Online, 1994.

99. Gray, P.; Yoffe, A. D.; Roselaar, L. Thermal Decomposition of the Nitroalkanes. *Transactions of the Faraday Society* **1955**, *51* (11), 1489-1497.

100. Wilde, K. A. Decomposition of Carbon-nitro Compounds. *Industrial & Engineering Chemistry* **1956**, *48* (4), 769-773.

101. Burch, R.; Breen, J. P.; Meunier, F. C. A Review of the Selective Reduction of NO_x with Hydrocarbons under Lean-burn Conditions with Non-zeolitic Oxide and Platinum Group Metal Catalysts. *Applied Catalysis B - Environmental* **2002**, *39* (4), 283-303.

102. Brosius, R.; Martens, J. A. Reaction Mechanisms of Lean-Burn Hydrocarbon SCR over Zeolite Catalysts: Scientific and Technical Developments in Automotive Emissions Control since the 1970s. *Topics in Catalysis* **2004**, *28* (1-4), 119-130.

103. Ding, S. D.; Bai, C. Y.; Liu, Z. P.; Wang, Y. Z. Enhanced Thermal Stability of Poly (p-dioxanone) in Melt by Adding an End-capping Reagent. *Journal of Thermal Analysis and Calorimetry* **2008**, *94* (1), 89-95.

104. Ando, T.; Fujimoto, Y.; Morisaki, S. Analysis of Differential Scanning Calorimetric Data for Reactive Chemicals. *Journal of Hazardous Materials* **1991**, *28* (3), 51-280.

105. Barton, J.; Rogers, R. *Chemical Reaction Hazards: A Guide to Safety*; The Institution of Chemical Engineers: Rugby, UK, 1994.

106. Keller, A.; Stark, D.; Fierz, H.; Heinzle, E.; Hungerbler, K. Estimation of the Time to Maximum Rate Using Dynamic DSC Experiments. *Journal of Loss Prevention in the Process Industries* **1997**, *10* (1), 31-41.

107. Kotsilkova, R.; Petkova, V.; Pelovski, Y. Thermal Analysis of Polymer-silicate Nanocomposites. *Journal of Thermal Analysis and Calorimetry* **2001**, *64* (2), 591-598.

108. Fogler, H. S. *Elements of Chemical Reaction Engineering*; Prentice-Hall: Englewood Cliffs, NJ, 1992.

109. Townsend, D. I.; Tou, J. C. Thermal Hazard Evaluation by an Accelerating Rate Calorimeter. *Thermochimica Acta* **1980**, *37* (1), 1-30.

110. Frank-Kamenetski, D. A. *Diffusion and Heat Transfer in Chemical Kinetics*; Plenum Press: New York, 1969.

111. Asatryan, R.; Bozzelli, J. W.; Simmie, J. M. Thermochemistry of Methyl and Ethyl Nitro, RNO_2, and Nitrite, RONO, Organic Compounds. *Journal of Physical Chemistry A* **2008**, *112* (14), 3172-3185.

112. Uchida, T.; Wakakura, M.; Miyake, A.; Ogawa, T. Thermal Decomposition of Organic Peroxide with Metals Using Calorimeters. *Journal of Thermal Analysis and Calorimetry* **2008**, *93* (1), 47-52.

113. Marco, E.; Cuartielles, S.; Pena, J. A.; Santamaria, J. Simulation of the Decomposition of Di-cumyl Peroxide in an ARSST Unit. *Thermochimica Acta* **2000**, *362* (1-2), 49-58.

114. Wei, C.; Saraf, S. R.; Rogers, W. J.; Mannan, M. S. Thermal Runaway Reaction Hazards and Mechanisms of Hydroxylamine with Acid/base Contaminants. *Journal of Hazardous Materials* **2004**, *421* (1-2), 1-9.

115. Li, X. R.; Koseki, H. SADT Prediction of Autocatalytic Material Using Isothermal Calorimetry Analysis. *Thermochimica Acta* **2005**, *431* (1-2), 113-116.

116. Lee, R. P.; Hou, H. Y.; Tseng, J. M.; Chang, M. K.; Shu, C. M. Reactive Incompatibility of DTBP Mixed with Two Acid Solutions. *Journal of Thermal Analysis and Calorimetry* **2008**, *93* (1), 269-274.

117. Stull, D. R. Linking Thermodynamics and Kinetics to Predict Real Chemical Hazards. *Journal of Chemical Education* **1974**, *51* (1), A21-A25.

VITA

Qingsheng Wang received his B.S., and M.S., in chemistry from Zhejiang University in 2003 and 2005, respectively. He entered the doctoral program in chemistry at Texas A&M University in August 2005 and switched to chemical engineering in August 2007 and graduated with his Ph.D. in August 2010. His research interests in the Mary Kay O'Connor Process Safety Center include process safety engineering, thermal analysis and calorimetry, chemical kinetics, and reaction engineering.

Dr. Wang has published 16 peer-reviewed journal papers and has more than 100 citations. He has presented his research at conferences including American Institue of Chemical Engineers (AIChE) Annual Meeting, Loss Prevention Symposium, and the American Chemical Society (ACS) Annual Meeting. Dr. Wang is an invited referee for 10 international journals, such as *Journal of Physical Chemistry B*, *Journal of Hazardous Materials*, *Materials Science and Engineering B*, and *Journal of Thermal Analysis and Calorimetry*.

Dr. Wang can be reached via the Mary Kay O'Connor Process Safety Center, Department of Chemical Engineering, Texas A&M University, 3122 TAMU, College Station, TX 77843-3122. His permanent email is: chemqswang@hotmail.com.